Phytochemistry 203 (2022) 113349

Contents lists available at ScienceDirect

Phytochemistry

journal homepage: www.elsevier.com/locate/phytochem

Bioactive molecular network-guided discovery of dihydro-β-agarofurans from the fruits of *Celastrus orbiculatus*

Jun Gu Kim [a], Thi Phuong Linh Le [a], Jae Sang Han [a], Yong Beom Cho [a], Haeun Kwon [b], Dongho Lee [b], Mi Kyeong Lee [b], Bang Yeon Hwang [a,*]

[a] College of Pharmacy, Chungbuk National University, Cheongju, 28160, South Korea
[b] Department of Plant Biotechnology, College of Life Sciences and Biotechnology, Korea University, Seoul, 02841, South Korea

ARTICLE INFO

Keywords:
Celastrus orbiculatus
Celastraceae
Dihydro-β-agarofuran sesquiterpenes
Molecular networking
Melanogenesis

ABSTRACT

A bioactive molecular networking strategy has been applied to discovery of bioactive constituents from the fruits of *Celastrus orbiculatus* Thunb., which showed significant inhibitory effects on the α-MSH-induced melanin production in B16F0 melanoma cells. In the obtained molecular network, the nodes with relatively high bioactive scores were prioritized for isolation; as a result, 12 undescribed dihydro-β-agarofuran sesquiterpenes together with 15 known compounds were isolated from MeOH extracts of the fruits of *C. orbiculatus*. Their structures were elucidated based on the interpretation of NMR, HRESIMS, ECD data, and single crystal X-ray diffraction. Among the obtained isolates, celastorbin A and (1*R*,2*S*,4*R*,5*S*,7*S*,8*S*,9*R*,10*S*)-1,2,8-triacetoxy-9-cinnamoyloxydihydro-β-agarofuran, which possessed high bioactive scores in the molecular network, exhibited potent inhibitory effects on the α-MSH-induced melanin production in B16F0 cells with IC_{50} values of 4.1 and 2.0 μM, respectively.

1. Introduction

Celastrus orbiculatus Thunb., which belongs to the Celastraceae family, is a rich source of dihydro-β-agarofuran derivatives, widely distributed in Korea, Japan, and mainland China. Various dihydro-β-agarofuran derivatives have been isolated from *C. orbiculatus* (Guo et al., 2004; Jin et al., 2002; Zhou et al., 2017, Zhu, et al., 2008) and other Celastraceae plants such as *C. paniculatus*, *C. flagellaris*, *C. angulatus*, *C. stephanotiifolius*, *C. monospermus*, *C. virens*, *Tripterygium willfordii*, *T. hypoglaucum*, and *Maytenus bilocularis* (Lu et al., 2006; Mu et al., 2021; Ning et al., 2015; Ning et al., 2022; Takaishi et al., 1990; Takaishi et al., 1993; Tu et al., 1992; Wibowo et al., 2016; Zheng et al., 2021). In addition, numerous biological activities of dihydro-β-agarofurans, such as cytotoxicity against tumor cells (Nunez et al., 2016; Zhu et al., 2008), inhibitory effect against osteoclastogenesis (Ning et al., 2022), reversal of multidrug resistance (Mu et al., 2021; Wibowo et al., 2016), anti-inflammation (Guo et al., 2004; Jin et al., ; 2002; Xu et al., 2012), and neuroprotection (Ning et al., 2015) were investigated. In the course of a research program aimed at discovering undescribed bioactive agents in medicinal plants, a MeOH extract as well as *n*-hexane, CH_2Cl_2, and ethylacetate fractions were examined to evaluate their inhibitory effects on the melanin production in α-melanocyte stimulating hormone (α-MSH) induced B16F0 melanoma cells. As a result, the *n*-hexane fraction of *C. orbiculatus* demonstrated significant inhibitory effect with an IC_{50} value of 33.1 μg/mL, and was selected for further isolation using a molecular networking technique based on liquid chromatography high-resolution mass spectrometry (LC-HRMS/MS) to avoid repeated isolation of hundreds of previously reported compounds.

MS/MS-based molecular networking (MN), which is publicly available via the Global Natural Products Social molecular networking (GNPS) web platform, has become a powerful strategy for the rapid and efficient dereplication and prioritization in natural product discovery. GNPS provides an open-access tool that uses a computational algorithm to compare large numbers of MS/MS spectra based on their cosine similarities. Related ions with similar MS/MS fragment patterns that cluster together can be visualized via MN (Quinn et al., 2017; Wang et al., 2016).

Feature based molecular networking (FBMN) includes the retention time and relative abundance of each ion in MN, and facilitates the discrimination of isomers with similar MS^2 patterns as compared to classical MN. (Nothias et al., 2020). In addition, the relationship between ions and their bioactivity can be expressed as a score based on the relative quantity of each ion, which allows prioritizing bioactive

* Corresponding author. College of Pharmacy Chungbuk National University Cheongju, 28160, South Korea
E-mail address: byhwang@chungbuk.ac.kr (B.Y. Hwang).

https://doi.org/10.1016/j.phytochem.2022.113349
Received 17 May 2022; Received in revised form 14 July 2022; Accepted 21 July 2022
Available online 13 August 2022
0031-9422/© 2022 Elsevier Ltd. All rights reserved.

compounds in the MN (Nothias et al., 2018).

In this study, the UHPLC-HRMS/MS-based bioactive molecular network was applied to an *n*-hexane fraction of *C. orbiculatus* using the FBMN method coupled with bioactivity measurements, resulting in the isolation of 12 undescribed dihydro-*β*-agarofuran sesquiterpenes along with 15 known compounds (Fig. 1). In addition, the bioactive molecular network-guided isolation and structures of compounds **1**–**12** as well as the structure-activity relationship (SAR) of the inhibitory effects on the melanin production in *α*-MSH-induced B16F0 melanoma cells were discussed.

2. Results and discussion

A FBMN was generated by performing an LC-HRMS/MS analysis of the silica gel chromatography subfraction of the *n*-hexane fraction of *C. orbiculatus*, after processing with the MZmine 2 software (see Materials and Methods and Table S1). The obtained relative amounts of all ions and observed inhibitory effects of each column fraction on the melanin production in α-MSH-induced B16F0 melanoma cells were uploaded to the workflow of the bioactive molecular network developed by Nothias et al. (https://github.com/DorresteinLaboratory/Bioactive_Molecular_Networks), and the bioactive score of each ion was calculated (Nothias et al., 2018). Moreover, the *in silico* fragmentation study tool, Network Annotation Propagation (NAP) (Kang et al., 2018), was used for dereplication using structure library of GNPS and SUPER NATRUAL II (SUPNAT) database (Banerjee et al., 2015). The bioactivity scores and structures predicted by the *in silico* tool were introduced to the generated FBMN, and the nodes with high bioactive scores ($r > 0.70$, p value < 0.03) are denoted by the red box to highlight a viable candidate for inhibiting melanin production (Fig. S1, Supporting Information). Most predicted node structures included dihydro-*β*-agarofuran derivatives; however, some nodes were different from those stored in the spectrum library or predicted *in silico*, while others did not have any spectral matches. The nodes with high bioactive scores were considered structurally unreported inhibitors of melanin production and selected for targeted isolation.

Compound **1** was represented by a node with the parent mass *m/z* 622.2999 and demonstrated the highest bioactive score in molecular network 1 ($r = 0.70$, p value $= 0.03$, MN 1, Fig. 2). The structure predicted by *in silico* analysis revealed the proton adduct of 1-acetoxy-8-(2-

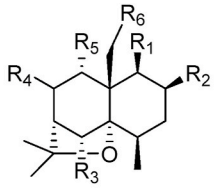

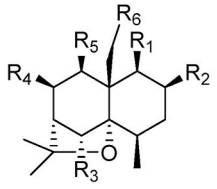

	R_1	R_2	R_3	R_4	R_5	R_6
1	AcO	H	*t*CinO	β-AcO	BzO	H
3	AcO	AcO	H	H	BzO	BzO
6	AcO	ButO	H	α-AcO	*t*CinO	H
7	AcO	AcO	AcO	α-AcO	*t*CinO	H
16	AcO	H	BzO	α-AcO	BzO	H
17	AcO	H	AcO	β-AcO	BzO	H
20	AcO	AcO	BzO	H	BzO	H
22	AcO	AcO	H	α-AcO	*t*CinO	H

	R_1	R_2	R_3	R_4	R_5	R_6
2	*t*CinO	H	AcO	BzO	BzO	H
4	BzO	H	AcO	HexO	BzO	H
5	OH	H	AcO	MeButO	BzO	H
8	BzO	OH	AcO	OH	BzO	H
9	AcO	AcO	AcO	OH	BzO	H
10	BzO	H	AcO	OH	BzO	AcO
11	BzO	H	AcO	AcetylHexO	BzO	H
12	BzO	BzO	AcO	MeButO	BzO	H
13	BzO	H	AcO	BzO	BzO	H
14	BzO	H	AcO	MeButO	BzO	H
15	BzO	H	AcO	ButO	BzO	H
18	AcO	H	AcO	BzO	BzO	H
19	BzO	H	AcO	AcO	BzO	H
21	AcO	HexO	H	AcO	*t*CinO	H
23	BzO	OH	AcO	BzO	BzO	H
24	BzO	BzO	AcO	AcO	BzO	H
25	AcO	BzO	AcO	BzO	BzO	H
26	BzO	BzO	AcO	BzO	BzO	H
27	AcO	AcO	AcO	BzO	BzO	H

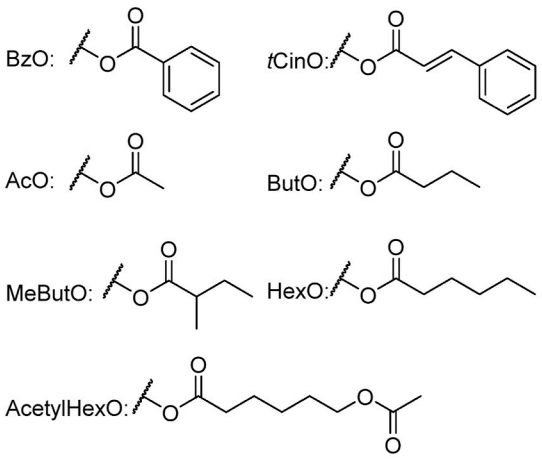

Fig. 1. Structures of compounds **1**–**27**.

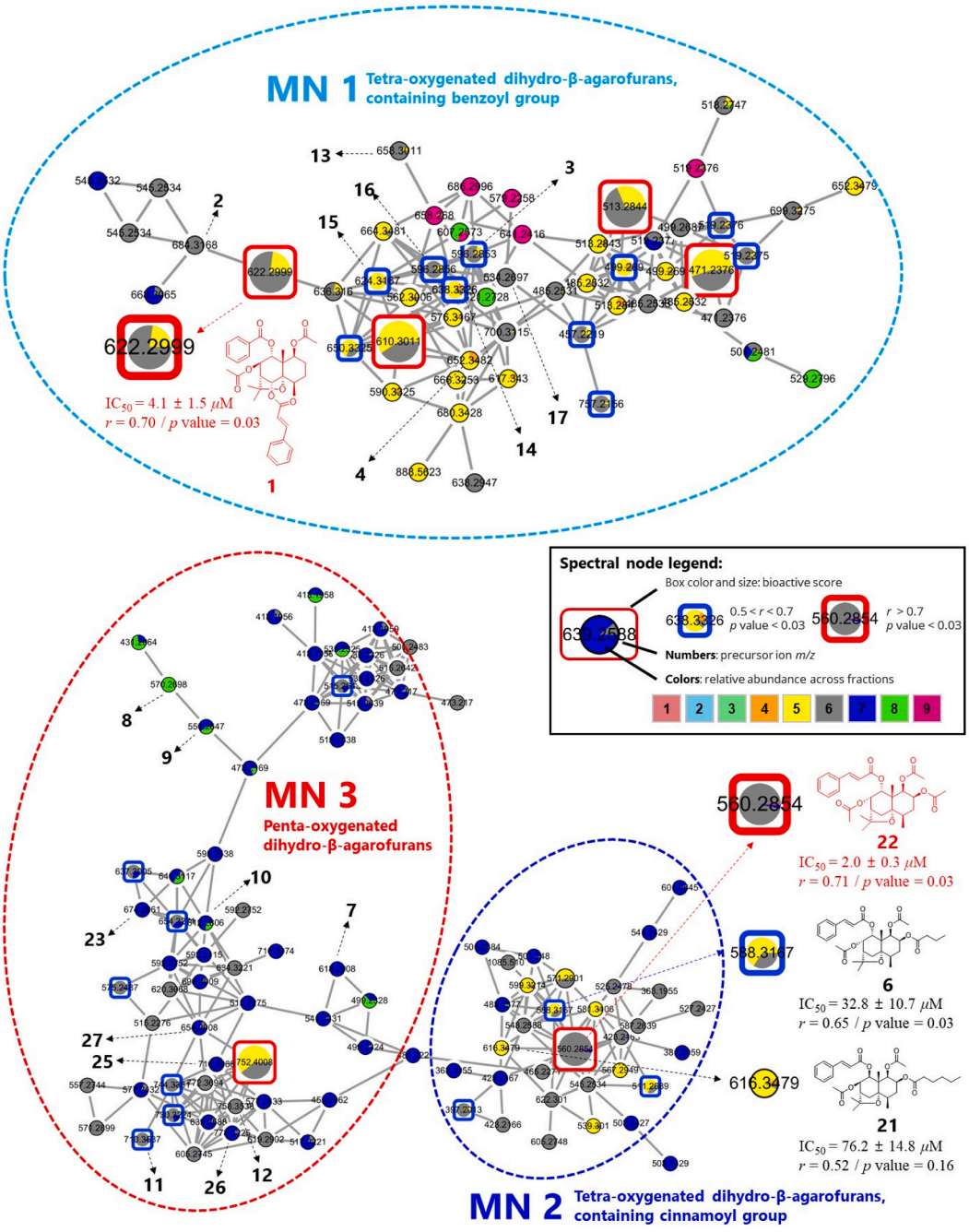

Fig. 2. Bioactivity-based molecular network (MN 1–3) and annotation of compounds **1**–**27**.

methylbutanoyloxy)-9-benzoyloxy-15-nicotinoyloxydihydro-*β*-agarofuran with the molecular formula of $C_{35}H_{43}NO_9$. However, the molecular formula identified by HRESIMS was $C_{35}H_{40}O_9$ (*m/z* 622.2999 $[M + NH_4]^+$; calcd 622.3011) with 16 indices of hydrogen deficiency showing a difference from the predicted structure. The ^{1}H NMR spectrum of **1** displayed four oxymethine protons at δ_H 5.85 (1H, s), 5.43 (1H, dd J = 4.3, 11.8 Hz), 5.29 (1H, d, J = 3.4 Hz), and 5.06 (1H, s); three tertiary methyl protons at δ_H 1.50 (3H, s), 1.49 (3H, s), and 1.46 (3H, s); and one secondary methyl proton at δ_H 1.06 (3H, d, J = 7.5 Hz), which represented typical proton signals of tetra-esterified dihydro-*β*-agarofuran. The remaining proton signals indicated the presence of a benzoyl group [δ_H 8.08 (2H, m), 7.56 (1H, m), 7.50 (2H, m)], a cinnamoyl group [δ_H 8.11 (2H, m), 7.72 (1H, d, J = 16.0 Hz), 7.61 (1H, m), 7.44 (2H, m), 6.46 (1H, d, J = 16.0 Hz)], and two acetyl groups [δ_H 1.60 (3H, s, Ac-1) and 2.26 (3H, s, Ac-8)]. The ^{13}C NMR and HSQC spectra exhibited 35 carbon signals, including four carbonyls, two olefinic carbons, twelve aromatic carbons, three quaternary carbons, six methines, two methylenes, and six methyl groups (Table 2). The positions of the ester groups were determined from the HMBC correlations between H-1 (δ_H 5.43) and the acetyl carbonyl carbon (δ_C 170.0), H-6 (δ_H 5.85) and the cinnamoyl carbonyl carbon (δ_C 166.8), H-8 (δ_H 5.29) and the acetyl carbonyl carbon (δ_C 169.5), and H-9 (δ_H 5.06) and the benzoyl carbonyl carbon (δ_C 166.5) (Fig. 3). The relative configuration of **1** was determined from the results of the ROESY experiment. The ROESY correlations between H-6/15-CH_3, H-9/15-CH_3, and 14-CH_3/15-CH_3 revealed the β-axial orientations of H-6, 14-CH_3, and 15-CH_3, and the α-orientations of both the 6-cinnamoyl and 9-benzoyl groups (Fig. 4). Further ROESY correlations of H-1/H-3α, and H-8/12-CH_3 suggested the β-orientation of the two acetyl groups at C-1 and C-8. The absolute configuration of **1** was determined by a dibenzoate chirality method, an

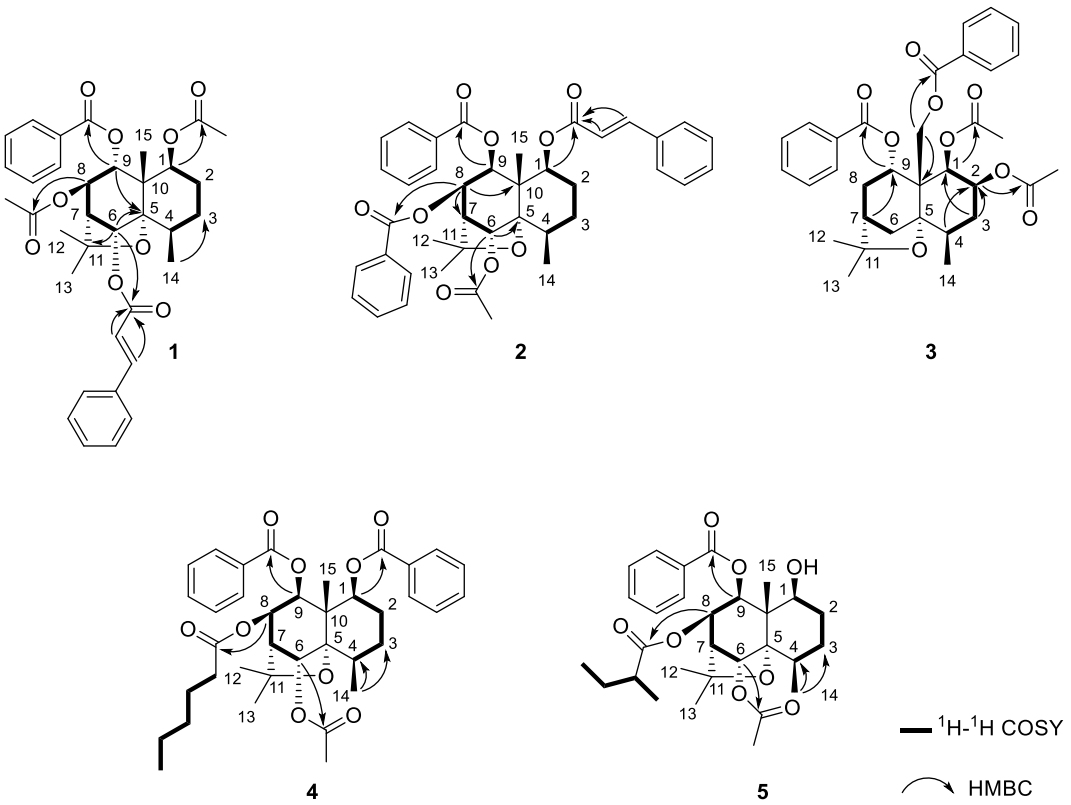

Fig. 3. Key HMBC and COSY correlations of compounds **1**–**5**.

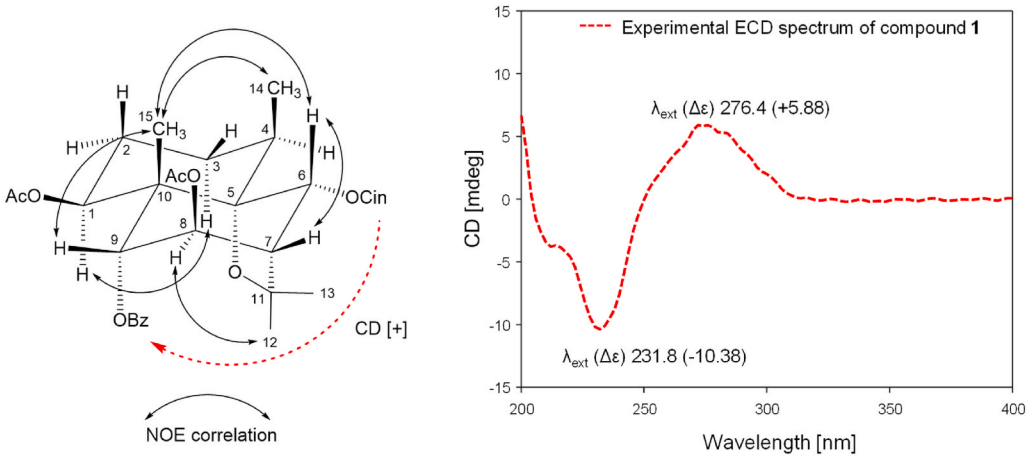

Fig. 4. Key ROESY correlations, ECD exciton coupling, and ECD spectrum of compound **1**.

extension of the circular dichroism exciton chirality procedure (Harada and Nakanishi, 1983). The first positive Cotton effect at 276.4 nm (Δε +5.88), and second negative Cotton effect at 231.8 nm (Δε −10.38) can be ascribed to the clockwise interaction of cinnamate at C-6α and benzoate at C-9α (Fig. 4). Additionally, the single-crystal X-ray diffraction analysis with Cu Kα radiation confirmed the absolute configuration of **1** as (1*S*,4*R*,5*S*,6*R*,7*R*,8*R*,9*R*,10*S*) [Flack parameter = 0.09 (11), and Hooft parameter = 0.12 (10)] (Fig. 5). Thus, the structure of **1** was determined as (1*S*,4*R*,5*S*,6*R*,7*R*,8*R*,9*R*,10*S*)-1,8-diacetyl-9-ben zoyloxy-6-cinnamyloxydihydro-*β*-agarofuran, and named as celastorbin A.

The difference between the structure predicted by NAP and the actual structure was caused by the lack of its ammonium adduct spectrum in the library (GNPS, SUPNAT2). Other nodes in molecular network 1 were further investigated for the isolation of undescribed compounds even those with moderate bioactive scores.

Compound **2** was present at the next node of **1** with a parent mass of *m/z* 684.3168 in the HRESIMS data ($C_{40}H_{46}NO_9$, $[M + NH_4]^+$; calcd 684.3167), which differed from that of **1** by 62.017 (Fig. 2). Along with the additional five aromatic protons and absence of one acetyl proton in the ^{1}H NMR spectrum, the observed *m/z* difference implies the conversion of an acetyl moiety into a benzoyl moiety. The positions of the four ester groups were determined by the observed HMBC correlations of H-1 (δ_H 5.41) and two olefinic protons (δ_H 7.25, 5.72) with the cinnamoyl carbonyl carbon (δ_C 166.1), H-6 (δ_H 6.22) with the acetyl carbonyl carbon (δ_C 170.0), H-8 (δ_H 5.82) with the benzoyl carbonyl carbon (δ_C 165.5), and H-9 (δ_H 5.74) with another benzoyl carbonyl carbon (δ_C 165.0) (Fig. 3). The relative configuration of **2** was

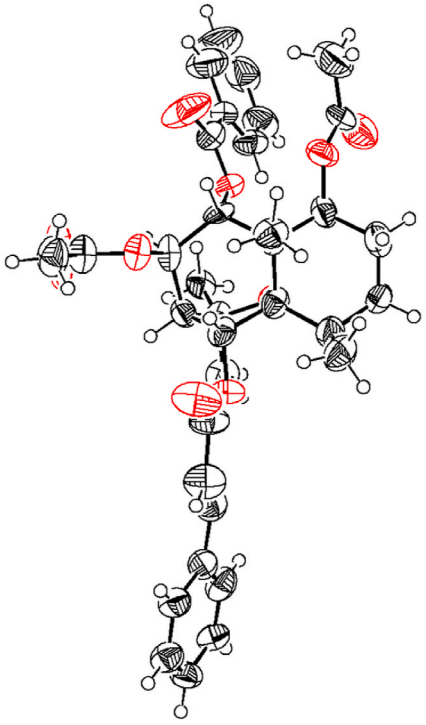

Fig. 5. X-ray ORTEP drawing of compound **1**.

determined by the ROESY experiment. The correlations between H-1/H-9, H-8/12-CH_3, and H-9/12-CH_3 revealed the β-orientations of the cinnamoyl and benzoyl groups. In addition, the ROESY correlations between the 6-axial proton and 14,15-axial methyl protons demonstrated the α-orientation the acetyl group at C-6 (Fig. S98, Supporting Information). The experimental ECD spectrum of **2** showed the first negative Cotton effect at 241 nm (Δε −33.28) and second positive Cotton effect at 225 nm (Δε +31.76), which matched well with those of the Davidoff-type split curve of (1*S*,4*R*,5*S*,6*R*,7*R*,8*R*,9*S*,10*S*)-6-acetoxy-1,8,9-tribenzoyloxydihydro-*β*-agarofuran (**13**, celafolin D-1), indicating that **2** possessed the same absolute configuration as **13** (Fig. S16) (Zhu et al., 2008). Thus, the structure of **2** was determined as (1*S*,4*R*,5*S*,6*R*,7*R*,8*R*,9*S*,10*S*)-6-acetoxy-8,9-dibenzoyloxy-1-cinnamyloxydihydro-*β*-agarofuran, and named as celastorbin B.

Compound **3** had the molecular formula $C_{33}H_{38}O_9$ serving as a node of its ammonium adduct with a parent mass of *m/z* 596.2853 ($C_{33}H_{42}NO_9$, $[M + NH_4]^+$; calcd 596.2854), which was located near the node of compound **1** (Fig. 2). The difference in *m/z* between **1** and **3** was 26.015, corresponding to a double bond, and the deficiency of olefinic protons and carbons in the ^1H and ^{13}C NMR spectra indicated that the cinnamoyl moiety of **1** was replaced with a benzoyl group in **3**. The locations of the two acetyl groups and two benzoyl groups were determined by the HMBC correlations between H-1 (δ_H 5.74) and the 1-acetyl carbonyl carbon (δ_C 169.6), H-2 (δ_H 5.62) and the 2-acetyl carbonyl carbon (δ_C 170.1), H-9 (δ_H 5.64) and the 9-benzoyl carbonyl carbon (δ_C 166.5), and H-15 (δ_H 5.06, 4.83) and the 15-benzoyl carbonyl carbon (δ_C 166.8) (Fig. 3). The relative orientations at C-1, C-4, C-9, and C-10 of **3** were identical to those of **1** based on the analysis of ROESY correlations (Fig. S98, Supporting Information). The observed ROESY correlations of H-2 (δ_H 5.62) with H-1 (δ_H 5.74), and 2-acetyl CH_3 (δ_H 2.09) with 15-CH_2 (δ_H 5.06 and 4.83) along with a small coupling constant between H-1 and H-2 ($J = 3.2$ Hz) corroborated that H-2 was equatorial, suggesting an β-orientation of the acetoxy group at C-2. The absolute configuration of compound **3** was determined by analyzing the experimental ECD data using dibenozate chirality method (Fig. S24, Supporting Information). Thus, the structure of **3** was determined as (1*R*,2*S*,4*R*,5*S*,7*R*,9*S*,10*R*)-1,2-diacetoxy-9,15-dibenzoyloxydihydro-*β*-agarofuran, and named as celastorbin C.

Compound **4** had a parent mass of *m/z* 652.3482 ($C_{37}H_{50}NO_9$, $[M + NH_4]^+$, calcd 652.3480), and the mass difference between **3** and **4** was 56.063, which corresponded to the C_4H_8 moiety. In addition, the hexanoyl peaks at δ_H 2.37 (2H, t, $J = 7.4$ Hz), 1.58 (2H, m), 1.26 (2H, m), 1.23 (2H, m), and 0.81 (3H, t, $J = 7.0$ Hz) in the ^1H NMR spectrum verified the replacement of the acetyl group in **3** by the hexanoyl moiety in **4**. The ^1H–^1H COSY data revealed the connectivity of H-1/H-2/H-3/H-4/H_3-14, H-6/H-7/H-8/H-9, and the hexanoyl H_2-2′/H_2-3′/H_2-4′/H_2-5′/H_3-6′ spin system. The positions of the ester functional groups were determined by the HMBC correlations from H-1 (δ_H 5.55) to the 1-benzoyl carbonyl carbon (δ_C 165.5), H-6 (δ_H 5.95) to the 6-acetyl carbonyl carbon (δ_C 169.9), H-8 (δ_H 5.54) to the hexanoyl carbonyl carbon (δ_C 172.5), and H-9 (δ_H 5.67) to another benzoyl carbonyl carbon (δ_C 164.8) (Fig. 3). The relative and absolute configuration of **4** established by the ROESY and its ECD spectrum, were similar to those of **2** (Figs. S32 and S98, Supporting Information). Consequently, the structure of **4** was determined as (1*S*,4*R*,5*S*,6*R*,7*R*,8*R*,9*S*,10*S*)-6-acetoxy-1,9-dibenzoyloxy-8-hexanoyloxydihydro-*β*-agarofuran, and named celastorbin D.

Compounds **1**–**5** also appeared as another cluster of sodium adducts in the molecular network, with some compounds preferred the cluster of sodium adduct ions over ammonium ions (Fig. S1). Compound **5**, which presented as a node of *m/z* 539.2614 ($[M + Na]^+$; calcd 539.2615), was obtained as an amorphous powder. Its ^1H NMR exhibited four oxymethine protons at δ_H 5.92 (1H, br s, H-6), 5.65 (1H, d, $J = 5.1$ Hz, H-9), 5.57 (1H, dd, $J = 4.4$, 5.1 Hz, H-8), and 4.10 (1H, dd, $J = 4.3$, 11.7 Hz, H-1), while the ^{13}C NMR showed three carbonyl carbons at δ_C 175.4, 169.8, and 165.8, which are characteristic of tri-esterified *β*-dihydroagarofuran with one hydroxy group (Tables 1 and 2). In addition, signals for a 2-methylbutanoyloxy group [2.42 (1H, sextet, $J = 7.0$ Hz), 1.68 (1H, m), 1.47 (1H, m), 1.15 (3H, d, $J = 7.0$ Hz), 0.80 (3H, t, $J = 7.4$ Hz); δ_C 175.4, 41.6, 26.6, 16.5, and 11.6)] were observed. The positions of the ester groups corresponded to those in the 6-acetoxy-9-benzoyl-8-(2-methylbutanoyloxy) structure determined by the HMBC correlations

Table 1
^1H NMR data for compounds **1**–**5** in $CDCl_3$ (*δ* in ppm, *J* in Hz)[a].

no.	1[b]	2[d]	3[e]	4[e]	5[c]
1	5.43 (dd, 4.3, 11.8)	5.41 (dd, 4.5, 11.6)	5.74 (d, 3.2)	5.55 (m)	4.10 (dd, 4.3, 11.7)
2	1.91 (m) 1.62 (m)	2.21 (m) 1.50 (m)	5.62 (q, 3.2)	1.78 (m) 1.23 (m)	1.63 (m) 1.52 (m)
3	2.26 (m) 1.47 (m)	1.80 (m) 1.71 (m)	2.55 (m) 1.82 (m)	2.21 (m) 1.50 (m)	2.03 (m) 1.44 (m)
4	2.37 (m)	2.28 (m)	2.01 (m)	2.27 (m)	2.19 (m)
5	–	–	–	–	–
6	5.85 (s)	6.22 (br s)	2.38 (m) 2.18 (m)	5.95 (s)	5.92 (br s)
7	2.58 (d, 3.3)	2.60 (d, 4.4)	2.16 (m)	2.51 (d, 4.3)	2.47 (d, 4.4)
8	5.29 (d, 3.4)	5.82 (dd, 4.4, 5.2)	2.46 (m) 2.19 (m)	5.54 (m)	5.57 (dd, 4.4, 5.1)
9	5.06 (s)	5.74 (d, 5.2)	5.64 (d, 7.1)	5.67 (d, 5.3)	5.65 (d, 5.1)
10	–	–	–	–	–
11	–	–	–	–	–
12	1.49 (s)	1.64 (s)	1.43 (s)	1.59 (s)	1.58 (s)
13	1.46 (s)	1.47 (s)	1.24 (s)	1.43 (s)	1.41 (s)
14	1.06 (d, 7.5)	1.11 (d, 7.4)	1.34 (d, 8.1)	1.10 (d, 7.5)	1.03 (d, 7.4)
15	1.50 (s)	1.61 (s)	5.06 (d, 12.5) 4.83 (d, 12.5)	1.62 (s)	1.42 (s)

[a] Assignments were based on the results of COSY, HSQC, and HMBC experiments. Signals of the ester substituents described in the Experimental Section.
[b] recorded in 500 MHz.
[c] recorded in 700 MHz.
[d] recorded in 800 MHz.
[e] recorded in 900 MHz.

Table 2
^{13}C NMR data for compounds **1**–**5** in $CDCl_3$ (δ in ppm)[a].

no.	1[b]	2[d]	3[e]	4[e]	5[c]
1	73.6	78.9	71.8	79.0	76.5
2	21.3	22.2	70.4	22.2	25.6
3	26.7	26.7	31.0	26.6	26.8
4	34.0	33.9	39.4	33.9	33.9
5	90.5	91.1	86.6	91.1	91.3
6	75.9	75.0	36.5	75.1	75.3
7	53.0	52.9	43.5	52.5	52.6
8	76.1	71.8	33.8	71.1	70.9
9	77.1	74.3	69.5	74.5	75.7
10	50.0	49.0	50.9	49.1	49.4
11	81.9	81.7	82.3	81.7	81.5
12	25.6	24.3	24.4	24.5	24.1
13	31.0	30.7	30.0	30.6	30.7
14	17.4	16.9	18.9	16.8	16.8
15	18.8	12.4	66.1	12.2	10.8

[a] Assignments were based on the results of COSY, HSQC, and HMBC experiments. Signals of the ester substituents described in the Experimental Section.
[b] recorded in 125 MHz.
[c] recorded in 175 MHz.
[d] recorded in 200 MHz.
[e] recorded in 225 MHz.

between the H-6 (δ_H 5.92)/6-acetyl carbonyl carbon (δ_C 169.8), H-8 (δ_H 5.57)/8-(2-methylbutyl) carbonyl carbon (δ_C 175.4), and H-9 (δ_H 5.65)/9-benzoyl carbonyl carbon (δ_C 165.8) (Fig. 3). The relative configuration of **5** was established as 6α-acetoxy-9β-benzoyloxy-8β-(2-methylbutanoyloxy)-1β-hydroxydihydro-*β*-agarofuran by the ROESY experiment (Fig. 6). Compound **5** has only one aromatic functionality; the dibenzoate chirality method could not be applied to determine its absolute configuration. Hence, ECD calculation was conducted, and the results were in good agreement with the experimental ECD spectrum of **5** (Fig. 6). Thus, the structure of **5** was determined as (1*S*,4*R*,5*S*,6*R*,7*R*,8*R*,9*S*,10*S*)-6-acetoxy-9-benzoyloxy-8-(2-methylbutanoyloxy)-1-hydroxydihydro-*β*-agarofuran, and named as celastorbin E.

In addition to the aforementioned clusters, a node with the parent mass *m/z* 560.2854, which demonstrated the highest bioactive score in molecular network 2 ($r = 0.71$, p value = 0.03, MN 2, Fig. 2), was isolated and identified as already known compound **22**. Further research on MN 2 was performed to isolate unrevealed bioactive compounds. Compound **6** presented as a node of parent mass with *m/z* 588.3167 ($C_{32}H_{46}NO_9$, $[M + NH_4]^+$; calcd 588.3167), which differed from that of compound **22** by 28.031 assigned to the C_2H_4 group. The proton signals of δ_H 2.26 (2H, t, $J = 7.3$ Hz), 1.65 (2H, m), and 0.94 (3H, t, $J = 7.4$ Hz) also revealed the butyrate moiety, and their connectivity was verified by the ^{1}H–^{1}H COSY spectrum (Fig. 7). The positions of the two acetyl groups were determined as C-1 and C-8 by the HMBC correlations between δ_H 5.53 (H-1) and δ_c 169.9 (1-acetyl carbonyl carbon), and between δ_H 5.39 (H-8) and δ_C 169.9 (8-acetyl carbonyl carbon). In addition, the HMBC correlations between δ_H 5.56 (H-2) and δ_C 172.7, and between δ_H 5.08 (H-9) and δ_C 166.3 established the position of the butanoyl group as C-2 and cinnamoyl group as C-9 (Fig. 7). Compound **7** was also detected near the node of **22** as a node with *m/z* 618.2908 ($C_{32}H_{46}NO_9$, $[M + NH_4]^+$; calcd 618.2909). Its ^{1}H NMR and ^{13}C NMR spectra were similar to those of **22**, except for the presence of an additional acetoxy group (Tables 3 and 4), which was consistent with the difference in the *m/z* value (58.006). The positions and relative configurations of all substituents of **7** determined by HMBC and ROESY experiments corresponded to the 1β,2β,6α,8α-tetraacetoxy-9α-cinnamyloxydihydro-*β*-agarofuran structure. (Figs. 6 and 7). The absolute configurations of **6** and **7** were deduced by comparing the experimental ECD spectrum with the calculated one (Fig. 6). Therefore, the structure of **6** (celastorbin F) and **7** (celastorbin G) were determined as (1*R*,2*S*,4*R*,5*S*,7*S*,8*S*,9*R*,10*S*)-1,8-diacetoxy-2-butanoyloxy-9-cinnamyloxydihydro-*β*-agarofuran and (1*R*,2*S*,4*R*,5*S*,6*R*,7*R*,8*S*,9*R*,10*S*)-1,2,6,8-tetraacettoxy-9-cinnamyloxydihydro-*β*-agarofuran, respectively.

Compounds **8**, **9**, and **10** had m/z values of 570.2698 ($[M + NH_4]^+$; calcd 570.2698), 550.2647 ($[M + NH_4]^+$; calcd 550.2647), and 612.2806 ($[M + NH_4]^+$; calcd 612.2803), respectively, in the nearby cluster (MN 3, Fig. 2). The ^{1}H NMR spectrum of **8** resembled that of **4**, except for the absence of a hexanoyl moiety and presence of an additional oxygenated methine proton (Table 5). The planar structure of **8** determined from the ^{13}C NMR and HMBC data, was 6-acetoxy-1,9-dibenzoyloxy-2,8-dihydroxydihydro-*β*-agarofuran (Table 6 and Fig. 7). Compound **9**, a neighboring node of **8**, presented five aromatic protons at δ_H 8.09 (2H, m), 7.60 (1H, m), and 7.49 (2H, m), and three acetyl protons at δ_H 2.14 (3H, s), 2.04 (3H, s), and 1.43 (3H, s) in the ^{1}H NMR spectrum, indicating the presence of one benzoyl and three acetyl groups. The positions of the substituent groups were determined by the HMBC correlations between H-1, H-2, and H-6 (δ_H 5.30, 5.39, and 6.17, respectively) and the acetyl carbonyl carbons (δ_C170.1, 170.0, and 169.8, respectively), as well as between H-9 (δ_H 5.38) and the benzoyl carbonyl carbon (δ_C 165.1) (Fig. 7). Compound **10** exhibited an additional *m/z* value of 42.011, indicating the presence of an acetoxy moiety instead of the hydroxyl group in **8**. The position of the acetyl group was determined by the HMBC correlation between H_2-15 (δ_H 5.08 and 4.81) and the acetyl carbonyl carbon (δ_C 170.5) (Fig. 7). The relative configurations of compounds **8**–**10** were determined by the ROESY experiments (Fig. S98). The absolute configuration of **8** and **10** was confirmed by the dibenzoate chirality method, which showed a Davidoff-type split curve with a first negative Cotton effect at 242 nm and second positive Cotton effect at 225 nm, due to the coupling of the two benzoyloxy functionalities at C-1 and C-9 (Figs. S64 and S80). The absolute configuration of **9** also characterized by comparison of experimental and calculated ECD data, due to the presence of only one benzoyl group in its structure (Fig. S72). Therefore, the structures of **8**, **9** and **10** were determined as (1*R*,2*S*,4*R*,5*S*,6*R*,7*R*,8*R*,9*S*,10*S*)-6-acetoxy-1,9-dibenzoyloxy-2,8-dihydroxydihydro-*β*-agarofuran (celastorbin H), (1*R*,2*S*,4*R*,5*S*,6*R*,7*R*,8*R*,9*S*,10*R*)-1,2,6-triacetoxy-9-benzoyloxy-8-hydroxydihydro-*β*-agarofuran (celastorbin I), and (1*S*,4*R*,5*S*,6*R*,7*R*,8*R*,9*S*,10*S*)-6,15-diacetoxy-1,9-dibenzoyloxy-8-hydroxydihydro-*β*-agarofuran (celastorbin J), respectively.

The nodes of compounds **11** and **12** with *m/z* values of 710.3537 and 758.3538, respectively, were located at some distances from those of **8**–**10** in the same cluster (MN 3, Fig. 2). The ^{1}H NMR spectrum of **11** is similar to that of **4**, except for the presence of an additional acetyl group (δ_H 2.02) and oxygenated methylene proton (δ_H 3.95), and the absence of a terminal triplet CH_3. The presence of an additional acetyl carbonyl carbon (δ_C 172.2) and an oxygenated methylene carbon (δ_H 64.3) in the ^{13}C NMR spectrum, and the difference of 58.005 Da in the HRESIMS data (*m/z* 710.3536, $[M + NH_4]^+$; calcd 710.3535) clearly confirmed the O-acetylation of the terminal methyl group in **4**. The ^{1}H–^{1}H COSY experiment verified the spin system of (6-O-acetyl)-hexanoyl groups, and the positions of all ester groups were determined by the HMBC data (Fig. 7). The relative and absolute configurations of **11** were determined by the ROESY and ECD experiments similar to those performed for **4** (Fig. S88). Therefore, the structure of **11** was determined as (1*S*,4*R*,5*S*,6*R*,7*R*,8*R*,9*S*,10*S*)-6-acetoxy-1,9-dibenzoyloxy-8-(6-acetyl)-hexanoyloxydihydro-*β*-agarofuran, and named as celastorbin K.

Compound **12** showed similar ^{1}H and ^{13}C NMR spectra with those of celafolin D-1 (**13**), except for the presence of an aliphatic ester group (Tables 5 and 6). The HRESIMS data of **12** (*m/z* 758.3537 $[M + NH_4]^+$; calcd 758.3535) was consistent with the molecular formula of $C_{43}H_{48}O_{11}$, and the difference in the *m/z* values of **12** and **13** corresponded to an additional $C_5H_8O_2$ group. A detailed analysis of the ^{1}H NMR spectrum showed a triplet methyl group at δ_H 0.76 (3H, t, $J = 7.4$ Hz), a doublet methyl group at δ_H 1.14 (3H, d, $J = 7.0$ Hz), a sextet methine proton at δ_H 2.39 (1H, sextet, $J = 7.0$ Hz), and the multiplet methylene protons at δ_H 1.65 and 1.45, suggested the presence of a 2-methylbutanoyl moiety. Further interpretation of the ^{13}C NMR data complemented by the HSQC and HMBC results indicated that **12** had the same planar structure as that of the recently reported *β*-dihydroagarofuran derivative, hypogricin I,

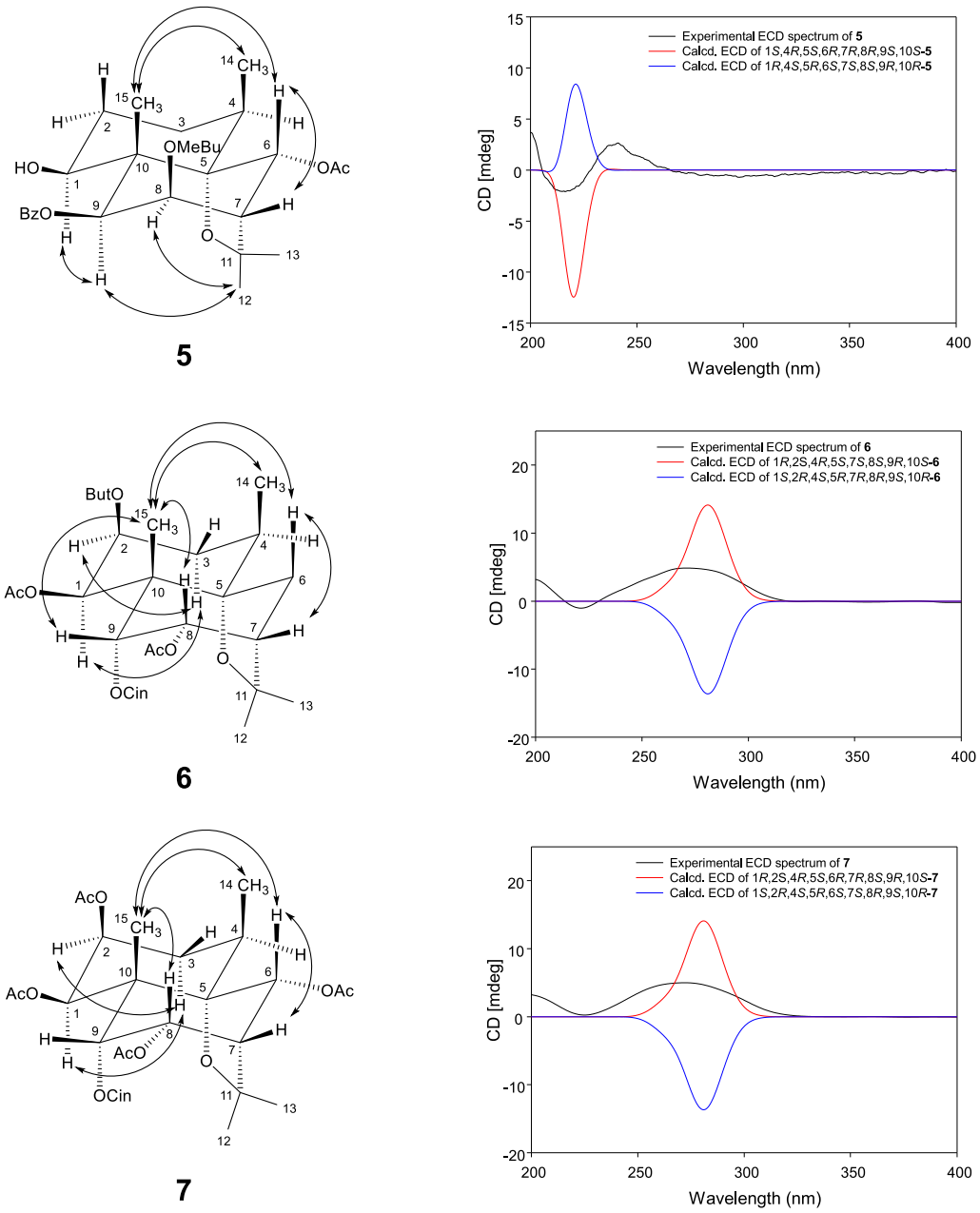

Fig. 6. Key ROESY correlations, and experimental and calculated ECD spectra of compounds **5**–**7.**

which was isolated from the twigs of *Tripterygium hypoglaucum* (Zheng et al., 2021). However, because the absolute configuration of hypogricin I was not identified, further stereochemical analyses were carried out in this study. The relative configuration obtained by ROESY experiment was 6α-acetoxy-1β,2β,9β-tribenzoyloxy-8β-(2-methylbutanoyloxy)-dihydro-*β*-agarofuran. As compared with hypogricin I, the relative configuration of 2-methylbutanoyloxy moiety had the β orientation at C-8, due to the correlation of H-8 (δ_H 5.61) with 12-CH_3 (δ_H 1.64) (Fig. 9). To verify the relative configuration of 2-methylbutyl group at C-8, single crystal X-ray diffraction analysis was conducted. (Fig. 8). However, the obtained Flack parameter [0.0 (3)] and the Hooft parameter [0.2 (19)] exhibited high standard deviations (0.3 and 0.19, respectively), which did not allow accurate determination of the absolute configuration of **12**. Hence, the dibenzoate chirality method was applied to the analysis of the ECD spectrum; the resulting absolute configuration was (1*R*,2*S*,4*R*,5*S*,6*R*,7*R*,8*R*,9*S*,10*S*) (Fig. 9). Therefore, the structure of **12** was determined as (1*R*,2*S*,4*R*,5*S*,6*R*,7*R*,8*R*,9*S*,10*S*)-6-acetoxy-1,2,9-tribezoyloxy-8-(2-methylbutanoyloxy)-dihydro-*β*-agarofuran, and named as celastorbin L. To elucidate the clustering mechanism of each molecular network, the nodes of each cluster were annotated with their structures. The 15 known compounds were identified as celafolin D-1 (**13**) (Takaishi et al., 1993), celafolin D-3 (**14**) (Takaishi et al., 1993), (1*S*,4*R*,5*S*,6*R*,7*R*,8*R*,9*S*,10*S*)-6-acetoxy-1,9-dibenzoyloxy-8-butyryloxydihydro-*β*-agarofuran (**15**) (Zhu et al., 2008) (1*S*,4*R*,5*S*,6*R*,7*R*,8*S*,9*R*,10*S*)-1,8-diacetoxy-6,9-dibenzoyloxydihydro-*β*-agarofuran (**16**) (Torres-Romero et al., 2009), celafolin C-1 (**17**) (Takaishi et al., 1993), (1*S*,4*R*,5*S*,6*R*,7*R*,8*S*,9*S*,10*S*)-1,6-diacetoxy-8,9-dibenzoyloxydihydro-*β*-agarofuran (**18**) (Takaishi et al., 1990), (1*S*,4*R*,5*S*,6*R*,7*R*,8*R*,9*S*,10*S*)-6,8-diacetoxy-1,9-dibenzoyloxydihydro-*β*-agarofuran (**19**) (Zhu et al., 2008), orbiculin A (**20**) (Kim et al., 1998), 1β,8β-diacetoxy-9β-cinnamoyloxy-2β-hexanoyloxy-*β*-dihydroagarofuran (**21**) (Guo et al., 2005), (1*R*,2*S*,4*R*,5*S*,7*S*,8*S*,9*R*,10*S*)-1,2,8-triacetoxy-9-cinnamoyloxydihydro-*β*-agarofuran (**22**) (Ning et al., 2015), triptogelin A-2 (**23**) (Takaishi et al., 1990), triptogelin A-11 (**24**) (Takaishi et al., 1991), (1*R*,2*S*,4*R*,5*S*,6*R*,7*R*,8*R*,9*S*,10*S*)-1,6-diacetoxy-3,8,9-tribezoyloxydihydro-*β*-agarofuran (**25**)

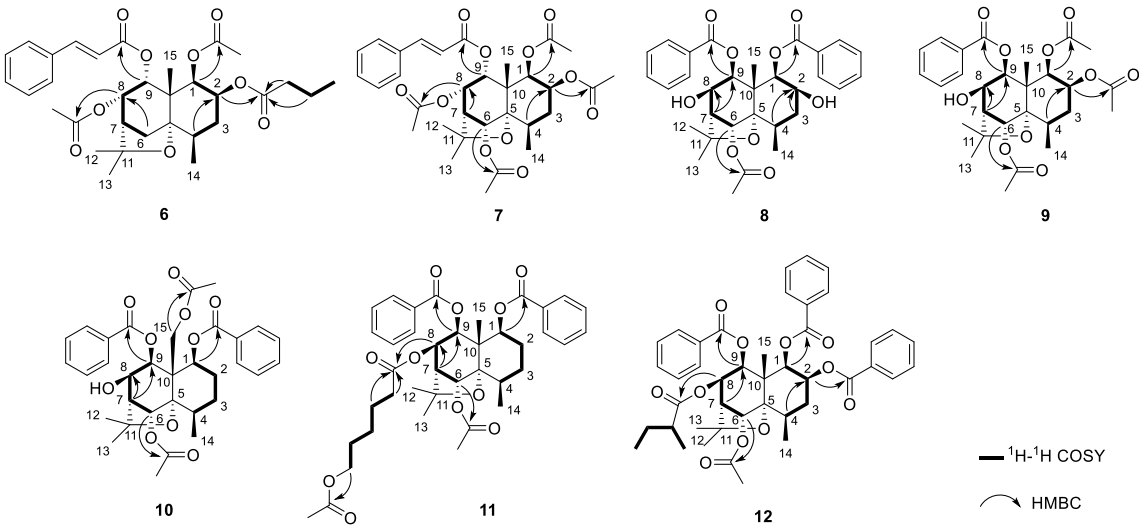

Fig. 7. Key HMBC and COSY correlations of compounds **6**–**12**.

Table 3
^{1}H NMR data for compounds **6**, **7**, and **22** in $CDCl_3$ (δ in ppm, J in Hz)[a].

no.	22[b]	6[c]	7[c]
1	5.53 (m)	5.53 (d, 3.7)	5.54 (m)
2	5.52 (m)	5.56 (q, 3.4)	5.56 (m)
3	2.42 (m) 1.78 (m)	2.41 (m) 1.75 (m)	2.38 (m) 1.79 (m)
4	1.93 (m)	1.92 (m)	2.32 (m)
5	–	–	–
6	2.27 (m) 2.17 (m)	2.25 (m) 2.15 (m)	5.39 (br s)
7	2.24 (m)	2.24 (m)	2.48 (m)
8	5.41 (dd, 2.9, 6.1)	5.39 (dd, 3.0, 6.1)	5.55 (m)
9	5.09 (d, 6.1)	5.08 (d, 6.1)	5.08 (d, 6.2)
10	–	–	–
11	–	–	–
12	1.55 (s)	1.54 (s)	1.58 (s)
13	1.22 (s)	1.22 (s)	1.41 (s)
14	1.26 (d, 8.0)	1.25 (d, 8.1)	1.20 (d, 7.6)
15	1.41 (s)	1.41 (s)	1.49 (s)

[a] Assignments were based on the results of COSY, HSQC, and HMBC experiments. Signals of the ester substituents described in the Experimental Section.
[b] recorded in 400 MHz.
[c] recorded in 900 MHz.

Table 4
^{13}C NMR data for compounds **6**, **7**, and **22** in $CDCl_3$ (δ in ppm)[a].

no.	22[b]	6[c]	7[c]
1	70.7	70.7	70.6
2	70.3	70.0	70.1
3	31.3	31.3	31.0
4	39.2	39.2	33.7
5	86.7	86.8	89.3
6	35.8	35.8	77.1
7	48.5	48.5	53.6
8	70.4	70.4	68.9
9	72.2	72.2	71.8
10	47.4	47.4	48.5
11	82.3	82.3	83.1
12	24.8	24.8	26.4
13	31.3	31.3	31.4
14	19.1	19.1	18.5
15	19.8	19.9	20.2

[a] Assignments were based on the results of COSY, HSQC, and HMBC experiments. Signals of the ester substituents described in the Experimental Section.
[b] recorded in 100 MHz.
[c] recorded in 225 MHz.

Table 5
^{1}H NMR data for compounds **8**–**12** in $CDCl_3$ (δ in ppm, J in Hz)[a].

no.	8[b]	9[b]	10[c]	11[b]	12[b]
1	5.58 (d, 3.6)	5.30 (d, 3.7)	5.77 (dd, 4.8, 12.0)	5.55 (m)	5.80 (d, 4.1)
2	4.29 (q, 3.1)	5.39 (q, 3.8)		1.80 (m)	5.76 (q, 3.3)
3	2.32 (m) 1.93 (m)	2.34 (m) 1.76 (m)		2.22 (m) 1.50 (m)	2.54 (m) 2.05 (m)
4	2.33 (m)	2.30 (m)	2.28 (m)	2.27 (m)	2.43 (m)
5	–	–	–	–	–
6	6.21 (br s)	6.17 (br s)	6.61 (br s)	5.93 (s)	6.09 (s)
7	2.55 (d, 4.2)	2.54 (d, 4.2)	2.44 (d, 4.0)	2.50 (d, 4.2)	2.55 (d, 4.1)
8	4.43 (t, 4.6)	4.39 (t, 4.5)	4.43 (m)	5.55 (m)	5.61 (t, 4.6)
9	5.49 (d, 5.0)	5.38 (d, 4.7)	5.67 (d, 5.4)	5.65 (d, 5.4)	5.65 (d, 5.4)
10	–	–	–	–	–
11	–	–	–	–	–
12	1.51 (s)	1.47 (s)	1.55 (s)	1.59 (s)	1.64 (s)
13	1.46 (s)	1.44 (s)	1.46 (s)	1.43 (s)	1.48 (s)
14	1.37 (d, 7.5)	1.25 (d, 7.4)	1.07 (d, 7.6)	1.09 (d, 7.5)	1.38 (d, 7.7)
15	1.88 (3H, s)	1.69 (s)	5.08 (d, 12.9) 4.81 (d, 12.9)	1.62 (s)	1.96 (s)

[a] Assignments were based on the results of COSY, HSQC, and HMBC experiments. Signals of the ester substituents described in the Experimental Section.
[b] recorded in 900 MHz.
[c] recorded in 700 MHz.

(Ning et al., 2015), triptogelin A-1 (**26**) (Takaishi et al., 1990), and 1β,2β, 6α-triacetoxy-8β,9β-dibenzoyloxy-dihydro-*β*-agarofuran (**27**) (Wu et al., 1992) by comparing their physicochemical and spectroscopic data with published values. After the annotation of isolated compounds **1**–**27** corresponding to various nodes of MN 1–3, the degree of oxygenation was found to be an important factor for clustering each network (Fig. 2). The MN 1 represent a cluster of the ammonium adducts of tetra-oxygenated dihydro-*β*-agarofuran derivatives that contain at least one benzoyl group. MN 2 and MN 3 comprise the networks of tetra-oxygenated dihydro-β-agarofurans containing cinnamoyl moiety (right, blue dotted circle) and penta-oxygenated dihydro-*β*-agarofurans (left, red dotted circle), respectively. Compound **7** (penta-esterified dihydro-*β*-agarofuran with a cinnamoyl group), which has only one more acetyl group than **8**, served as a bridge between the two sub-clusters MN 2 and MN 3. Thus, Compounds **12** and **13** (celafolin D-1) have similar structures, except for the presence of a 2-methylbutanoyl moiety in **12**, but appeared in different clusters.

Table 6
^{13}C NMR data for compounds **8**–**12** in $CDCl_3$ (δ in ppm)[a].

no.	8[b]	9[b]	10[c]	11[b]	12[b]
1	79.3	76.5	79.0	79.0	76.3
2	69.7	69.7	23.3	22.4	70.9
3	32.5	31.1	26.4	26.6	31.2
4	33.6	33.5	33.2	33.9	33.4
5	91.6	90.9	90.7	91.1	90.8
6	74.6	74.5	73.9	75.1	74.8
7	54.3	54.2	55.4	52.5	52.7
8	70.1	70.3	68.8	71.2	70.8
9	77.1	76.8	75.3	74.5	75.0
10	49.0	48.5	51.9	49.2	48.8
11	81.5	81.5	81.2	81.7	82.1
12	24.1	24.1	24.4	24.1	24.2
13	30.8	30.7	30.5	30.6	30.7
14	18.7	18.2	15.6	16.8	18.5
15	14.7	14.0	60.7	12.2	14.1

[a] Assignments were based on the results of COSY, HSQC, and HMBC experiments. Signals of the ester substituents described in the Experimental Section.
[b] recorded in 225 MHz.
[c] recorded in 175 MHz.

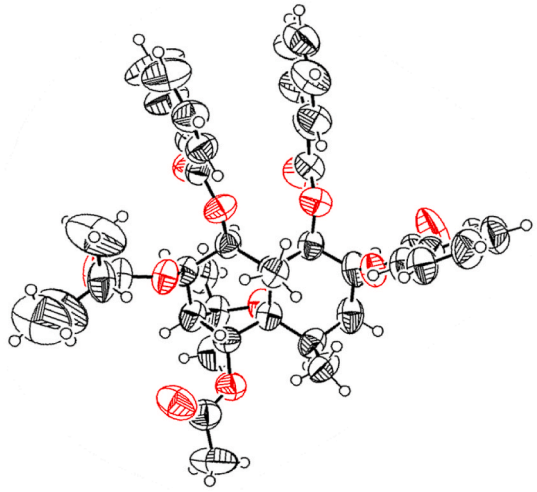

Fig. 8. X-ray ORTEP drawing of compound **12**.

All compounds were tested for their inhibitory effects on the α-MSH-induced melanin production in B16F0 melanoma cells, using arbutin as a positive control (Table 7). The cytotoxicity of the isolated compounds was tested with an MTT reagent, and none of the test compounds demonstrated significant cytotoxicity at their effective concentrations for the inhibition of melanin production (Figs. S99 and S100, Supporting Information). As expected, the node at *m/z* 622.2999 ($r = 0.70$, $p = 0.03$) in cluster MN 1, which was identified as compound **1**, exhibited a strong inhibitory effect on melanin production with an IC_{50} value of 4.1 ± 1.5 μM. The two nodes at *m/z* 638.3326 (compound **14**) and 624.3167 (compound **15**) with bioactive scores of $0.5 < r < 0.7$, exhibited significant inhibitory effects with IC_{50} values of 31.3 ± 13.3 and 38.8 ± 0.7 μM, respectively. The node at *m/z* 710.3537 (compound **11**) in MN 3 also showed a significant inhibitory effect with an IC_{50} value of 36.7 ± 8.1 μM. The node at *m/z* = 560.2854 (compound **22**) in MN 2 with the highest score ($r = 0.71$, $p = 0.03$), also demonstrated a strong inhibitory effect (IC_{50} = 2.0 ± 0.3 μM), which was consistent with the bioactive score obtained by bioactive molecular network at the fractionation stage. Two related nodes at *m/z* 588.3167 (compound **6**) and 616.3479 (compound **21**), which clustered with compound **22**, were also identified as the structurally related tetra-oxygenated dihydro-*β*-agarofurans with different bioactive scores. A comparison of the inhibitory effects of compounds **6** (IC_{50} = 32.8 ± 10.7 μM, butanoyl moiety at C-2) and **21** (IC_{50} = 76.2 ± 14.8 μM, hexanoyl moiety at C-2) indicated that increasing the carbon chain length at C-2 ester moiety decreased the inhibitory effects on melanin production. The bioactive scores obtained for compounds **22** ($r = 0.71$, $p = 0.03$), **6** ($r = 0.65$, $p = 0.06$), and **21** ($r = 0.52$, $p = 0.15$) were strongly correlated with the experimental IC_{50} values against melanin production. These results confirmed that the bioactive molecular network-based strategy was highly efficient for the prediction and targeted isolation of melanin production inhibitors.

Table 7
Inhibitory effects of compounds **1**–**27** on the α-MSH-induced melanin production in B16F0 melanoma cells[a].

Compound	IC_{50} (μM)	Compound	IC_{50} (μM)
1	4.1 ± 1.5	**15**	38.8 ± 0.7
2	75.3 ± 8.9	**16**	78.3 ± 1.1
3	>100	**17**	>100
4	>100	**18**	76.3 ± 29.0
5	50.5 ± 6.4	**19**	36.2 ± 16.6
6	32.8 ± 10.7	**20**	>100
7	61.2 ± 6.1	**21**	76.2 ± 14.8
8	33.8 ± 5.1	**22**	2.0 ± 0.3
9	71.6 ± 6.1	**23**	>100
10	54.2 ± 0.8	**24**	75.1 ± 14.2
11	36.7 ± 8.1	**25**	33.5 ± 10.8
12	82.7 ± 1.9	**26**	>100
13	>100	**27**	>100
14	31.3 ± 13.3	**Arbutin**[b]	85.0 ± 6.8

[a] Results are expressed as the mean IC_{50} values in μM obtained from triplicate experiments.
[b] Arbutin was used as positive control.

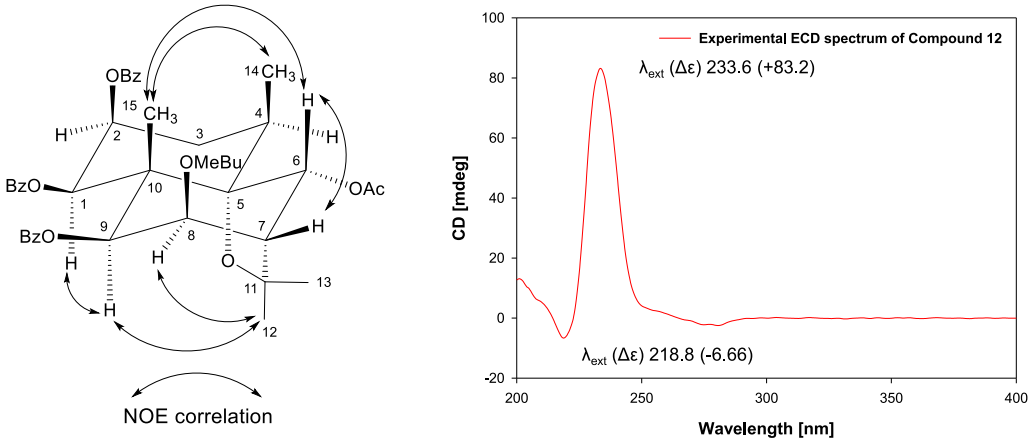

Fig. 9. Key ROESY correlations and ECD spectrum of compound **12**.

3. Conclusions

In our current study, the bioactive molecular network was organized for the discovery of dihydro-β-agarofuran sesquiterpenes from the fruits of *C. orbiculatus*. It was clustered by the degree of esterification level, and the isolated dihydro-β-agarofuran compounds **1**–**27** were annotated. The molecular network and spectra of each isolate were uploaded to the GNPS web platform to be applied for further study on plants of the Celastraceae family. The targeted compounds, which possessed high bioactive scores in molecular network, exhibited strong inhibitory effects on the melanin production in B16F0 melanoma cells. Therefore, the dihydro-β-agarofuran sesquiterpenes isolated from the fruits of *C. orbiculatus* have potential for melanogenesis inhibitors, but further studies on their mechanism of action are needed.

4. Experimental

4.1. General methods

Optical rotations were determined on a JASCO DIP-1000 polarimeter. UV and IR spectra were obtained using a JASCO UV-550 spectrophotometer and JASCO FT-IR 4100 spectrometer, respectively. ECD spectra were acquired on a JASCO J-715 spectrometer. NMR spectra were recorded on a Bruker AVANCE 400, 500, 700, 800, and 900 MHz spectrometers using $CDCl_3$ solvent. HRESIMS and UHPLC-HRMS/MS analyses were performed utilizing an Orbitrap Exploris 120 mass spectrometer coupled with Vanquish UHPLC system (ThermoFisher Scientific). Chromatographic elution was conducted using a YMC Triart C18 (100 × 2.1 mm, 1.9 μm, 0.3 mL/min) column at a temperature of 30 °C, with a mobile phase consisting of water + 0.1% formic acid (A) and CH_3CN + 0.1% formic acid (B) and linear gradient of 10–100% B (0–15 min). Mass detection was performed in the *m/z* range of 200–2000, and the resolution of the Orbitrap mass analyzer was fixed at 60,000 for the full MS scan, and 15,000 for the data-dependent MS^n scan. The following parameters were used during MS measurements: a spray voltage of 3.5/2.5 kV for the positive/negative modes, ion transfer tube temperature of 320 °C, HESI probe vaporizer temperature of 275 °C, RF lens 70 (%). Ultra-pure nitrogen (>99.999%) was used as both the sheath and auxiliary gas for the HESI probe, and set to 50 arb and 15 arb, respectively. The normalized higher-energy collision dissociation (HCD) energy of 30% was utilized for the collision of ions in the Orbitrap detector. MS/MS fragmentation was performed in the data-dependent MS^n mode to obtain an MS^2 spectrum of the four most intense ions, with a dynamic exclusion filter to exclude the repeated fragmentation of ions within 2.5 s after acquiring the MS^2 spectrum. Column chromatography was performed using silica gel (Merck, 70–230 mesh) and Sephadex LH-20 (25–100 μm, Pharmacia) column. Medium pressure liquid chromatography (MPLC) was performed on a Biotage Isolera Prime chromatography system with Lichroprep RP-18 (Merck, 40–63 μm). Preparative HPLC was conducted using a Waters HPLC system equipped with two Waters 515 pumps, a 2996 photodiode-array detector, and a YMC J'sphere ODS H-80 column (4 μm, 150 × 20 mm, i. d., flow rate: 6.0 mL/min). Thin layer chromatography was performed using precoated silica gel 60 F_{254} (0.25 mm, Merck) plates, and spots were detected by a 10% vanillin-H_2SO_4 aqueous spray reagent.

4.2. Plant material

Dried fruits of *Celastrus orbiculatus* Thunb. (Celastraceae) were purchased from the Kyungdong herbal market (Seoul, South Korea) in January 2020 and identified by one of the authors (B. Y. H). A voucher specimen (CBNU-2020-01-CO) was deposited at the Herbarium of the College of Pharmacy, Chungbuk National University, South Korea.

4.3. Feature based molecular networking (FBMN)

The MS/MS data were processed by the MZmine 2.53 software using the ADAP algorithm (Pluskal et al., 2010) for chromatogram building and deconvolution (detailed parameters for the MZmine processing are described in the Supporting Information, Table S1). The processed data (MGF format) were uploaded to GNPS (http://gnps.ucsd.edu) for the FBMN. The product ion and fragment ion mass tolerances were set to 0.02 Da. The edge between the nodes was created when they exhibited cosine scores above 0.7 and more than six matched peaks. Furthermore, these edges were kept in the network if and only if each of the nodes appeared in each other's respective top 10 most similar nodes. The created network (https://gnps.ucsd.edu/ProteoSAFe/status.jsp?task=562c59ab966d4e1b9a6174ec8ba45fcb) was downloaded and visualized by Cytoscape 3.8.2 (Shannon et al., 2003).

The results of the relative quantification of ions, processed by MZmine (CSV format), were modified based on their bioactivity (reflecting the inhibitory effects on melanin production), and uploaded to 'Bioactive Molecular Networks' workflow (https://github.com/DorresteinLaboratory/Bioactive_Molecular_Networks). As a result, a table containing the Pearson correlation value (*r* value) between the quantity of ions and their bioactivity, and its significance (*p* value) was obtained. The Network Annotation Propagation (NAP) tool in the GNPS web platform was utilized for the *in silico* analysis of the molecular network. The following parameters were used for this purpose: first 10 candidates, mass tolerance of 5 ppm, database of GNPS and SUPNAT2 (Supernatural II). The bioactive scores and predicted structures determined by this method were directly imported to the molecular network using the Cytoscape software. The filter function of Cytoscape was utilized to highlight the nodes with $r > 0.70$ and p value < 0.03 (red), and $0.50 < r < 0.70$ and p value < 0.03 (blue). In addition, the chemViz 2 plugin in Cytoscape was used to visualize the predicted structure of each node.

4.4. Extraction and isolation

The dried fruits of *C. orbiculatus* (3.0 kg) were extracted with MeOH (3 × 18 L) by maceration for 3 days at room temperature (25 °C), filtered, and evaporated under a reduced pressure to obtain a MeOH extract. A suspension of the extract (395 g) in distilled water was partitioned sequentially with *n*-hexane (2 × 2 L), CH_2Cl_2 (2 × 2 L), EtOAc (2 × 2 L), and *n*-BuOH (2 × 2 L). The *n*-hexane-soluble fraction (186 g) was subjected to silica gel column chromatography and eluted using an *n*-hexane-acetone gradient system (50:1 to 0:1) to yield nine fractions (COFH1 – COFH9). COFH5 (21.9 g) was further separated by silica gel column chromatography with an *n*-hexane-ethylacetate (10:1 to 8:1) mixture to obtain seven fractions (COFH5-1 – COFH5-7). COFH 5–2 (1.9 g) was separated by RP-MPLC with a MeOH–H_2O (60:40 to 100:0) gradient system to yield eight subfractions (COFH5-2-1 – COFH 5-2-8). Subfraction COFH5-2-5 (211.5 mg) was isolated by preparative HPLC (MeCN–H_2O, 92:8, isocratic) to yield compounds **14** (t_R = 32.1 min, 17.4 mg) and **4** (t_R = 39.2 min, 1.5 mg). COFH 5–4 (5.6 g) was isolated by RP-MPLC and eluted with a MeOH–H_2O gradient system (70:30 to 100:0) to obtain seven subfractions (COFH5-4-1 – COFH5-4-7). Subfraction COFH5-4-3 (640.0 mg) was subjected to RP-MPLC, using a MeOH–H_2O (70:30) isocratic system and separated into two fractions (COFH5-4-3-4 and COFH5-4-3-5). The fraction COFH5-4-3-4 (526.4 mg) was further purified by preparative HPLC (MeCN–H_2O, 87:13, isocratic) to yield compounds **16** (t_R = 28.1 min, 3.9 mg), **1** (t_R = 32.1 min, 1.4 mg), and **15** (t_R = 40.0 min, 20.2 mg). The fraction COFH5-4-3-5 (46.7 mg) was isolated by preparative HPLC (MeCN–H_2O, 90:10, isocratic) to obtain compound **21** (t_R = 43.8 min, 0.96 mg). COFH 5-5 (7.0 g) was isolated by RP-MPLC using a MeOH–H_2O gradient system (60:40 to 100:0) to afford compound **17** (67.0 mg). COFH 5–6 (1.6 g) was subjected to RP-MPLC and eluted with a MeOH–H_2O gradient system (60:40 to 100:0) to obtain four subfractions (COFH5-6-1 – COFH5-6-4). Subfraction COFH5-6-4 (104.8 mg) was isolated by preparative HPLC

(MeCN–H_2O, 80:20, isocratic) to obtain compounds **6** (t_R = 37.3 min, 1.5 mg), **20** (t_R = 38.2 min, 20.8 mg), **3** (t_R = 39.8 min, 2.5 mg), and **19** (t_R = 45.1 min, 11.0 mg). COFH 6 (18.9 g) was subjected to silica gel column chromatography and eluted with an *n*-hexane-ethylacetate (8:1) isocratic system to yield nine fractions (COFH6-1 – COFH6-9). COFH 6–4 (1.9 g) was isolated by RP-MPLC with a MeOH–H_2O gradient system (70:30 to 100:0) to obtain ten subfractions (COFH6-4-1 – COFH6-4-10). Subfraction COFH6-4-2 (138.6 mg) was purified by preparative HPLC (MeCN–H_2O, 67:33, isocratic) to afford compound **5** (t_R = 56.7 min, 6.0 mg). Subfraction COFH6-4-3 (813.8 mg) was further isolated by RP-MPLC using a MeOH–H_2O (70:30) isocratic eluent, yielding nine subfractions (COFH6-4-3-1 – COFH6-4-3-9). COFH6-4-3-5 (384.8 mg) was isolated by preparative HPLC (MeCN–H_2O, 75:25, isocratic) to afford compound **18** (t_R = 56.5 min, 22.8 mg). COFH6-4-4 (535.8 mg) was isolated by preparative HPLC (MeCN–H_2O, 85:15) to obtain compounds **13** (t_R = 32.0 min, 43.0 mg), **2** (t_R = 36.2 min, 2.0 mg), and **12** (t_R = 38.0 min, 5.9 mg). COFH 6–7 (7.0 g) was isolated by RP-MPLC with a MeOH–H_2O gradient system (60:40 to 100:0) to yield seven subfractions (COFH6-7-1 – COFH6-7-7). COFH6-7-3 (4.6 g) was isolated by preparative HPLC (MeCN–H_2O, 70:30, isocratic) to afford compound **22** (t_R = 34.5min, 32.9 mg). COFH6-7-5 (676.4 mg) was purified by preparative HPLC (MeCN–H_2O, 82:18, isocratic) to obtain compounds **11** (t_R = 33.8 min, 4.5 mg) and **26** (t_R = 40.5 min, 10.8 mg). COFH 6–9 (1.5 g) was isolated by RP-MPLC with a MeOH–H_2O gradient system (55:45 to 100:0) to obtain six subfractions (COFH6-9-1 – COFH6-9-6). COFH6-9-4 (110.0 mg) was purified by preparative HPLC (MeCN–H_2O, 65:35, isocratic) to obtain compound **7** (t_R = 58.0 min, 6.5 mg). COFH 7 (5.4 g) was subjected to RP-MPLC and eluted with a MeOH–H_2O step gradient system (50:50 to 100:0) to yield 13 subfractions (COFH7-1 – COFH7-13). COFH 7–6 (114.8 mg) was isolated by preparative HPLC (MeCN–H_2O, 55:45, isocratic) to obtain compounds **8** (t_R = 55.8 min, 1.4 mg) and **9** (t_R = 53.2 min, 2.3 mg). COFH 7–9 (671.9 mg) was purified by preparative HPLC (MeCN–H_2O, 60:40, isocratic) to obtain compounds **10** (t_R = 21.7 min, 1.0 mg), **23** (t_R = 22.8 min, 4.7 mg), and **27** (t_R = 24.0 min, 3.5 mg). COFH 7–10 (300.5 mg) was isolated by preparative HPLC (MeCN–H_2O, 70:30, isocratic) to yield compounds **25** (t_R = 40.0 min, 0.8 mg) and **24** (t_R = 44.2 min, 3.0 mg).

4.4.1. Celastorbin A (1)

Transparent orthorhombic crystal; $[\alpha]_D^{25}$ +51 (*c* 1.0, MeOH); UV (MeOH) λ_{max} (log ε) 220 (3.79), 280 (4.02) nm; ECD (MeOH, *c* 1.0) λ_{max} ($\Delta\varepsilon$) 276 (+5.88), 232 (−10.38) nm; ^{1}H NMR (500 MHz, $CDCl_3$) δ_H 1.60 (3H, s, Ac-1), *trans*-OCin-6 [8.11 (2H, m), 7.72 (1H, d, *J* = 16.0 Hz), 7.61 (1H, m), 7.44 (2H, m), 6.46 (1H, d, *J* = 16.0 Hz)], 2.26 (3H, s, Ac-8), OBz-9 [8.08 (2H, m), 7.56 (1H, m), 7.50 (2H, m)], and others in Table 1; ^{13}C NMR (125 MHz, $CDCl_3$) δ_C Ac-1 (170.0, 20.9), *trans*-OCin-6 (166.8, 145.7, 133.3, 129.6 × 2, 129.5, 128.3 × 2, 117.7), Ac-8 (169.5, 21.2), OBz-9 (166.5, 133.3, 130.1 × 2, 130.0, 128.7 × 2), and others in Table 2; HRESIMS *m/z* 622.2994 $[M + NH_4]^+$ (calcd for $C_{35}H_{44}O_9N$, 622.3011).

4.4.2. Celastorbin B (2)

White amorphous powder; $[\alpha]_D^{25}$ −30 (*c* 0.5, MeOH); UV (MeOH) λ_{max} (log ε) 228 (3.50), 274.2 (1.11) nm; ECD (MeOH, *c* 1.0) λ_{max} ($\Delta\varepsilon$) 241 (−33.28), 225 (+31.76) nm; ^{1}H NMR (800 MHz, $CDCl_3$) δ_H *trans*-OCin-1 [7.25 (1H, d, *J* = 16.0 Hz), 7.23 (1H, m), 7.17 (2H, m), 6.91 (2H, m), 5.72 (1H, d, *J* = 16.0 Hz)], 2.13 (3H, s, Ac-6), OBz-8 [8.08 (2H, m), 7.58 (1H, m), 7.48 (2H, m)], OBz-9 [7.77 (2H, m), 7.22 (1H, m), 7.08 (2H, m)] and others in Table 1; ^{13}C NMR (200 MHz, $CDCl_3$) δ_C *trans*-OCin-1 (166.1, 144.1, 134.1, 129.8, 128.3 × 2, 127.8 × 2, 118.1), Ac-6 (170.0, 21.3), OBz-8 (165.5, 133.1, 130.1, 129.8 × 2, 128.6 × 2), OBz-9 (165.0, 132.5, 129.9, 129.6 × 2, 128.1 × 2), and others in Table 2; HRESIMS *m/z* 684.3168 $[M + NH_4]^+$ (calcd for $C_{40}H_{46}O_9N$, 684.3167).

4.4.3. Celastorbin C (3)

White amorphous powder; $[\alpha]_D^{25}$ +14 (*c* 0.3, MeOH); UV (MeOH) λ_{max} (log ε) 231 (2.78), 274 (0.88) nm; ECD (MeOH, *c* 1.0) λ_{max} ($\Delta\varepsilon$) 234 (+14.67), 214 (+0.80) nm; ^{1}H NMR (900 MHz, $CDCl_3$) δ_H 1.58 (3H, s, Ac-1), 2.09 (3H, s, Ac-2), OBz-9 [8.08 (2H, m), 7.56 (1H, m), 7.50 (2H, m)], OBz-15 [8.11 (2H, m), 7.61 (1H, m), 7.44 (2H, m)] and others in Table 1;^{13}C NMR (225 MHz, $CDCl_3$) δ_C Ac-1 (169.6, 20.5), Ac-2 (170.1, 21.4), OBz-9 (166.5, 133.3, 130.1 × 2, 130.0, 128.7 × 2), OBz-15 (166.8, 133.3, 129.6 × 2, 129.5 × 2, 128.3), and others in Table 2; HRESIMS *m/z* 596.2853 $[M + NH_4]^+$ (calcd for $C_{33}H_{42}O_9N$, 596.2854).

4.4.4. Celastorbin D (4)

White amorphous powder; $[\alpha]_D^{25}$ −34 (*c* 0.3, MeOH); UV (MeOH) λ_{max} (log ε) 228 (2.84), 274 (0.89) nm; ECD (MeOH, *c* 1.0) λ_{max} ($\Delta\varepsilon$) 241 (−8.24), 214 (+17.14) nm; ^{1}H NMR (900 MHz, $CDCl_3$) δ_H OBz-1 [7.62 (2H, m), 7.18 (1H, m), 6.92 (2H, m)], 2.12 (3H, s, Ac-6), OHex-8 [2.37 (2H, t, *J* = 7.4 Hz), 1.58 (2H, m), 1.26 (2H, m), 1.23 (2H, m), 0.81 (3H, t, *J* = 7.0 Hz)], OBz-9 [7.60 (2H, m), 7.32 (1H, m), 7.10 (2H, m)] and others in Table 1; and ^{13}C NMR (225 MHz, $CDCl_3$) δ_C OBz-1 (165.5, 132.2, 129.9, 129.2 × 2, 127.6 × 2), Ac-6 (169.9, 21.3), OHex-8 (172.5, 34.5, 31.2, 24.1, 22.4, 13.8), OBz-9 (164.8, 132.5, 129.6, 129.1 × 2, 127.8 × 2), and others in Table 2; HRESIMS *m/z* 652.3481 $[M + NH_4]^+$ (calcd for $C_{37}H_{50}O_9N$, 652.3480).

4.4.5. Celastorbin E (5)

White amorphous powder; $[\alpha]_D^{25}$ −55 (*c* 0.3, MeOH); UV (MeOH) λ_{max} (log ε) 229 (3.08), 273 (0.97) nm; ECD (MeOH, *c* 1.0) λ_{max} ($\Delta\varepsilon$) 241 (+3.43), 216 (+0.13) nm; ^{1}H NMR (700 MHz, $CDCl_3$) δ_H 2.10 (3H, s, Ac-6), OMeBut-8 [2.42 (1H, sextet, *J* = 7.0 Hz), 1.68 (1H, m), 1.47 (1H, m), 1.15 (3H, d, *J* = 7.0 Hz), 0.80 (3H, t, *J* = 7.4 Hz)], OBz-9 [7.99 (2H, m), 7.54 (1H, m), 7.41 (2H, m)] and others in Table 1; ^{13}C NMR (175 MHz, $CDCl_3$) δ_C Ac-6 (169.8, 21.3), OMeBut-8 (175.4, 41.6, 26.6, 16.5, 11.6), OBz-9 (165.8, 133.2, 130.0, 129.6 × 2, 128.4 × 2), and others in Table 2; HRESIMS *m/z* 539.2614 $[M + Na]^+$ (calcd for $C_{29}H_{40}NaO_8$, 539.2615).

4.4.6. Celastorbin F (6)

White amorphous powder; $[\alpha]_D^{25}$ +5 (*c* 0.3, MeOH); UV (MeOH) λ_{max} (log ε) 218 (3.64), 280 (4.46) nm; ECD (MeOH, *c* 1.0) λ_{max} ($\Delta\varepsilon$) 271 (+4.87), 221 (−1.04) nm; ^{1}H NMR (900 MHz, $CDCl_3$) δ_H 1.95 (3H, s, Ac-1), OBut-2 [2.26 (2H, t, *J* = 7.3 Hz), 1.65 (2H, m), 0.94 (3H, d, *J* = 7.4 Hz)], 1.82 (3H, s, Ac-8), *trans*-OCin-9 [7.69 (1H, d, *J* = 16.0 Hz), 7.56 (2H, m), 7.39 (2H, m), 7.38 (1H, m), 6.45 (1H, d, *J* = 16.0 Hz)], and others in Table 3; ^{13}C NMR (225 MHz, $CDCl_3$) δ_C Ac-1 (169.9, 20.9), OBut-2 (172.7, 36.7, 18.4, 13.6), Ac-8 (169.9, 20.6), *trans*-OCin-9 (166.3, 145.2, 134.4, 130.3, 128.8 × 2, 128.3 × 2, 117.9), and others in Table 4; HRESIMS *m/z* 588.3166 $[M + NH_4]^+$ (calcd for $C_{32}H_{46}O_9N$, 588.3167).

4.4.7. Celastorbin G (7)

White amorphous powder; $[\alpha]_D^{25}$ +4 (*c* 0.3, MeOH); UV (MeOH) λ_{max} (log ε) 218 (2.46), 281 (3.48) nm; ECD (MeOH, *c* 1.0) λ_{max} ($\Delta\varepsilon$) 272 (+5.02), 225 (+0.25) nm; ^{1}H NMR (900 MHz, $CDCl_3$) δ_H 2.04 (3H, s, Ac-1), 1.94 (3H, s, Ac-2), 2.12 (3H, s, Ac-6), 1.81 (3H, s, Ac-8), *trans*-OCin-9 [7.69 (1H, d, *J* = 16.0 Hz), 7.56 (2H, m), 7.39 (3H, m), 6.41 (1H, d, *J* = 16.0 Hz)], and others in Table 3; ^{13}C NMR (225 MHz, $CDCl_3$) δ_C Ac-1 (170.1, 21.3), Ac-2 (169.2, 20.8), Ac-6 (169.6, 21.3), Ac-8 (169.9, 20.6), *trans*-OCin-9 (166.0, 145.6, 134.3, 130.1, 128.9 × 2, 128.4 × 2, 117.6), and others in Table 4; HRESIMS *m/z* 618.2906 $[M + NH_4]^+$ (calcd for $C_{32}H_{44}O_{11}N$, 618.2909).

4.4.8. Celastorbin H (8)

White amorphous powder; $[\alpha]_D^{25}$ −41 (*c* 0.5, MeOH); UV (MeOH) λ_{max} (log ε) 229 (2.40), 273 (0.76) nm; ECD (MeOH, *c* 1.0) λ_{max} ($\Delta\varepsilon$) 242 (−6.97), 225 (+12.88) nm; ^{1}H NMR (900 MHz, $CDCl_3$) δ_H OBz-1 [7.68 (2H, m), 7.23 (1H, m), 6.98 (2H, m)], 2.15 (3H, s, Ac-6), OBz-9 [7.67 (2H, m), 7.36 (1H, m), 7.13 (2H, m)], and others in Table 5; ^{13}C NMR (225 MHz, $CDCl_3$) δ_C OBz-1 (165.2, 132.7, 129.3 × 2, 129.2, 127.8 × 2), Ac-6 (170.0, 21.5), OBz-9 (165.0, 132.9, 129.6, 129.3 × 2, 128.1 × 2),

and others in Table 6; HRESIMS *m/z* 570.2695 $[M + NH_4]^+$ (calcd for $C_{31}H_{40}O_9N$, 570.2698).

4.4.9. Celastorbin I (9)

White amorphous powder; $[\alpha]_D^{25}$ −3 (*c* 0.5, MeOH); UV (MeOH) λ_{max} (log ε) 231 (2.20), 274 (0.70) nm; ECD (MeOH, *c* 1.0) λ_{max} ($\Delta\varepsilon$) 237 (−6.27), 220 (−1.54) nm; ^{1}H NMR (900 MHz, $CDCl_3$) δ_H 2.04 (3H, s, Ac-1), 1.43 (3H, s, Ac-2), 2.14 (3H, s, Ac-6), OBz-9 [8.09 (2H, m), 7.60 (1H, m), 7.49 (2H, m)], and others in Table 5; ^{13}C NMR (225 MHz, $CDCl_3$) δ_C Ac-1 (170.1, 21.4), Ac-2 (170.0, 20.5), Ac-6 (169.8, 21.4), OBz-9 (165.1, 133.6, 129.8, 129.7 × 2, 128.7 × 2), and others in Table 6; HRESIMS *m/z* 550.2646 $[M + NH_4]^+$ (calcd for $C_{28}H_{40}O_{10}N$, 550.2647).

4.4.10. Celastorbin J (10)

White amorphous powder; $[\alpha]_D^{25}$ −54 (*c* 0.5, MeOH); UV (MeOH) λ_{max} (log ε) 229 (2.06), 274 (0.65) nm; ECD (MeOH, *c* 1.0) λ_{max} ($\Delta\varepsilon$) 242 (−5.17), 225 (+7.43) nm; ^{1}H NMR (700 MHz, $CDCl_3$) δ_H OBz-1 [7.62 (2H, m), 7.18 (1H, m), 6.91 (2H, m)], 2.13 (3H, s, Ac-6), OBz-9 [7.68 (2H, m), 7.39 (1H, m), 7.20 (2H, m)], 2.34 (3H, s, Ac-15), and others in Table 5; ^{13}C NMR (175 MHz, $CDCl_3$) δ_C OBz-1 (165.4, 132.5, 129.3, 129.2 × 2, 127.7 × 2], Ac-6 (169.8, 21.4), OBz-9 (164.7, 132.9, 129.3, 129.4 × 2, 128.2 × 2), Ac-15 (170.5, 21.3), and others in Table 6; HRESIMS *m/z* 612.2803 $[M + NH_4]^+$ (calcd for $C_{33}H_{42}O_{10}N$, 612.2803).

4.4.11. Celastorbin K (11)

White amorphous powder; $[\alpha]_D^{25}$ −35 (*c* 0.3, MeOH); UV (MeOH) λ_{max} (log ε) 225 (3.26), 270 (1.03) nm; ECD (MeOH, *c* 0.5) λ_{max} ($\Delta\varepsilon$) 250 (−0.06), 221 (+1.44) nm; ^{1}H NMR (900 MHz, $CDCl_3$) δ_H OBz-1 [7.61 (2H, m), 7.18 (1H, m), 6.92 (2H, m)], 2.12 (3H, s, Ac-6), O-AcetylHex-8 [3.95 (2H, m), 2.39 (2H, m), 2.02 (3H, s), 1.61 (2H, m), 1.55 (2H, m), 1.30 (2H, m)], OBz-9 [7.60 (2H, m), 7.32 (1H, m), 7.10 (2H, m)] and others in Table 5; ^{13}C NMR (225 MHz, $CDCl_3$) δ_C OBz-1 (165.5, 132.2, 129.9, 129.2 × 2, 127.6 × 2), Ac-6 (169.9, 21.3), O-AcetylHex-8 (172.2, 171.1, 64.3, 34.3, 28.2, 25.5, 24.4, 21.0), OBz-9 (164.8, 132.5, 129.6, 129.2 × 2, 127.9 × 2), and others in Table 6; HRESIMS *m/z* 710.3536 $[M + NH_4]^+$ (calcd for $C_{39}H_{52}O_{11}N$, 710.3535).

4.4.12. Celastorbin L (12)

Colorless monoclinic crystal; $[\alpha]_D^{25}$ +34 (*c* 0.5, MeOH); λ_{max} (log ε) 228 (3.45), 274.2 (1.09) nm; ECD (MeOH, *c* 1.0) λ_{max} ($\Delta\varepsilon$) 233 (+83.2), 220 (−6.66) nm; ^{1}H NMR (900 MHz, $CDCl_3$) δ_H OBz-1 [7.50 (2H, m), 7.13 (1H, m), 6.86 (2H, m)], OBz-2 [8.02 (2H, m), 7.60 (1H, m), 7.48 (2H, m)], 2.14 (3H, s, Ac-6), OMeBut-8 [2.39 (1H, sextet, J = 7.0 Hz), 1.65 (1H, m), 1.45 (1H, m), 1.14 (3H, d, J = 7.0 Hz), 0.76 (3H, t, J = 7.4 Hz)], OBz-9 [7.57 (2H, m), 7.25 (1H, m), 7.03 (2H, m)] and others in Table 5; ^{13}C NMR (225 MHz, $CDCl_3$) δ_C OBz-1 (165.3, 132.3, 129.2 × 2, 129.1, 127.6 × 2), Ac-6 (169.8, 21.4), OBz-2 (165.9, 133.0, 130.3, 129.6 × 2, 128.6 × 2), OMeBut-8 (175.1,41.6, 26.6, 16.5, 11.6), OBz-9 (165.0, 132.5, 129.9, 129.6 × 2, 128.1 × 2), and others in Table 6; HRESIMS *m/z* 758.3537 $[M + NH_4]^+$ (calcd for $C_{43}H_{52}O_{11}N$, 758.3535).

4.5. ECD computational calculation method

The preliminary geometries of compounds **5**–**7**, and **9** were obtained by the Chem3D 20.1.1 software and the corresponding conformers were searched using the procedure implemented in Spartan '20 software under the MMFF force field (Wavefunction Inc.: Irvine, CA, 2013). Either a systematic search method or Monte Carlo method was used for the conformer search within a global minimum of 10 kJ/mol. Selected conformers were further optimized by density functional theory (DFT) calculations conducted at the B3LYP/6-31+G(d) level using the Gaussian 16 W package (Frisch et al., 2016). Time-dependent DFT ECD calculations of the optimized conformers were performed at the B3LYP/6–31+G (2d,p) level using a CPCM solvent model in MeOH. The overall calculated curves were obtained as the sum of Gaussian functions in accordance with Boltzmann weighting after UV correction and visualized via SpecDis 1.71 (Bruhn et al., 2017).

4.6. X-ray crystallographic analysis of compounds 1 and 12

Single crystals of compounds **1** and **12** were obtained in MeOH by vapor diffusion. The X-ray crystallographic data were collected on a Bruker D8 Venture diffractometer equipped with a monochromatic fine-focus Cu Kα (λ = 1.54178 Å) radiation source. Data were collected by a PHOTON 100 CMOS detector at 223(2) K with the APEX2 software (Bruker AXS Inc.). The full-matrix least-squares refinement of the crystal structure was performed using the SHELXL-2014 computer program (Sheldrick, 2015). Further analysis of single crystal properties was conducted by the PLATON software (Spek, 2015). Molecular graphics were computed using the Mercury 4.2 software. Crystallographic data for **1** and **12** were deposited at the Cambridge Crystallographic Data Centre (CCDC; deposition number: CCDC 2158631 and CCDC 2158627). Copies of these data can be obtained free of charge from the CCDC at www.ccdc.cam.ac.uk.

4.6.1. Crystal data of celastorbin A (1)

$C_{35}H_{40}O_9$, M_r = 604.67, size 0.317 × 0.161 × 0.136 mm^3, a = 12.664 (2) Å, b = 14.527(2) Å, c = 17.353(3) Å, α = 90.00°, β = 90.00°, γ = 90.00°, V = 3193.4(9) Å^3, T = 223(2) K, Space group $P2_12_12_1$, Z = 4, μ = 0.740 mm^{-1}; 18,586 collected reflections, 5641 independent reflections (R_{int} = 0.0474), R_1 (all data) = 0.1248, wR_2 (all data) = 0.3153. The absolute structure was determined using the Flack parameter x = 0.09(11) and by performing a Bijvoet pair analysis involving the Hooft method (Hooft y = 0.12(10), P2 (true) = 1.00, P3 (true) = 0.999, P3 (racemic-twin) = 0.001).

4.6.2. Crystal data of celastorbin L (12)

$C_{43}H_{48}O_{11}$, M_r = 740.81, size 0.343 × 0.060 × 0.057 mm^3, a = 12.4689(18) Å, b = 14.4411(19) Å, c = 23.151(3) Å, α = 90.00°, β = 101.097 (7)°, γ = 90.00°, V = 4090.8(10) Å^3, T = 223(2) K, Space group $P2_1$, Z = 4, μ = 0.708 mm^{-1}; 72,537 collected reflections, 16,532 independent reflections (R_{int} = 0.1247), R_1 (all data) = 0.1940, wR_2 (all data) = 0.3537. The absolute structure was determined using the Flack parameter x = 0.0 (3) and by performing a Bijvoet pair analysis involving the Hooft method (Hooft y = 0.20(19), P2 (true) = 1.00, P3 (true) = 0.684, P3 (racemic-twin) = 0.316).

4.7. Measurement of α-MSH induced melanin production and cell viability

B16F0 melanoma cells were seeded into 96-well tissue culture plates at a density of 3 × 10^3 cells/mL, and stimulated with 10 nM of α-MSH in the presence or absence of compounds. Arbutin was used as a positive control. After incubation at 37 °C for 72 h, absorbance was measured at a wavelength of 405 nm against a calibration curve prepared using melanin standards, to determine the quantity of extracellular melanin in the culture supernatant. The viability of the remaining cells was determined by an MTT-based colorimetric assay (Sigma Chemical Co., St. Louis, MO) (Yun et al., 2018).

Declaration of competing interest

The authors declare that they have no known competing financial interests or personal relationships that could have appeared to influence the work reported in this paper.

Data availability

The authors do not have permission to share data.

Acknowledgements

This study was supported by a National Research Foundation of Korea (NRF) grant funded by the Korean government (MIST) (No. 2020R1A2C1008406). The authors wish to thank the Korea Basic Science Institute for the NMR spectroscopic measurements.

Appendix A. Supplementary data

Supplementary data to this article can be found online at https://doi.org/10.1016/j.phytochem.2022.113349.

References

Banerjee, P., Erehman, J., Gohlke, B.O., Wilhelm, T., Preissner, R., Dunkel, M., 2015. Super Natural II – a database of natural products. Nucleic Acids Res. 43, D935–D939. https://doi.org/10.1093/nar/gku886.

Bruhn, T., Schaumlöffel, A., Hemberger, Y., Pecitelli, G., 2017. SpecDis version 1.71, Berlin, Germany.

Frisch, M.J., Trucks, G.W., Schlegel, H.B., Scuseria, G.E., Robb, M.A., Cheeseman, J.R., Scalmani, G., Barone, V., Petersson, G.A., Nakatsuji, H., Li, X., Caricato, M., Marenich, A.V., Bloino, J., Janesko, B.G., Gomperts, R., Mennucci, B., Hratchian, H. P., Ortiz, J.V., Izmaylov, A.F., Sonnenberg, J.L., Williams-Young, D., Ding, F., Lipparini, F., Egidi, F., Goings, J., Peng, B., Petrone, A., Henderson, T., Ranasinghe, D., Zakrzewski, V.G., Gao, J., Rega, N., Zheng, G., Liang, W., Hada, M., Ehara, M., Toyota, K., Fukuda, R., Hasegawa, J., Ishida, M., Nakajima, T., Honda, Y., Kitao, O., Nakai, H., Vreven, T., Throssell, K., Montgomery Jr., J.A., Peralta, J.E., Ogliaro, F., Bearpark, M.J., Heyd, J.J., Brothers, E.N., Kudin, K.N., Staroverov, V.N., Keith, T.A., Kobayashi, R., Normand, J., Raghavachari, K., Rendell, A.P., Burant, J. C., Iyengar, S.S., Tomasi, J., Cossi, M., Millam, J.M., Klene, M., Adamo, C., Cammi, R., Ochterski, J.W., Martin, R.L., Morokuma, K., Farkas, O., Foresman, J.B., Fox, D.J., 2016. Gaussian 16, Revision B.01. Gaussian, Inc., Wallingford CT, USA.

Guo, Y.Q., Li, X., Xu, J., Li, N., Meng, D.L., Wang, J.H., 2004. Sesquiterpene esters from the fruits of *Celastrus orbiculatus*. Chem. Pharm. Bull. 52, 1134–1136. https://doi.org/10.1248/cpb.52.1134.

Guo, Y.Q., Li, X., Xu, J., Meng, D.L., Li, Y.S., Ohizumi, Y., 2005. Sesquiterpene esters from the fruits of *Celastrus orbiculatus*. Chem. Lett. 34, 764–765. https://doi.org/10.1246/cl.2005.764.

Harada, N., Nakanishi, K., 1983. Circular Dichroic Spectroscopy: Exciton Coupling in Organic Stereochemistry. University Science Books, Mill Valley, CA, USA.

Jin, H.J., Hwang, B.Y., Kim, H.S., Lee, J.H., Kim, Y.H., Lee, J.J., 2002. Antiinflammatory constituents of *Celastrus orbiculatus* inhibit the NF-κB activation and NO production. J. Nat. Prod. 65, 89–91. https://doi.org/10.1021/np010428r.

Kang, K.B., Park, E.J., da Silva, R.R., Kim, H.W., Dorrestein, P.C., Sung, S.H., 2018. Targeted isolation of neuroprotective dicoumaroyl neolignans and lignans from *Sageretia theezans* using *in Silico* molecular network annotation propagation-based dereplication. J. Nat. Prod. 81, 1819–1828. https://doi.org/10.1021/acs.jnatprod.8b00292.

Kim, S.E., Kim, Y.H., Kim, Y.C., Lee, J.J., 1998. A new sesquiterpene ester from *Celastrus orbiculatus* reversing multidrug resistance in cancer cells. J. Nat. Prod. 61, 108–111. https://doi.org/10.1021/np9702392.

Lu, Y., Yang, S., Zou, Z., Luo, X., Chen, H., Xu, L., 2006. Evoninoate sesquiterpene alkaloids from the stem of *Celastrus paniculatus*. Heterocycles 68, 1241–1247.

Mu, H., Tang, S., Zuo, Q., Huang, M., Zhao, W., 2021. Dihydro-β-agarofuran-type sesquiterpenoids from the seeds of *Celastrus virens* and their multidrug resistance reversal activity against the KB/VCR cell line. J. Nat. Prod. 84, 588–600. https://doi.org/10.1021/acs.jnatprod.0c01182.

Ning, R., Lei, Y., Liu, S., Wang, H., Zhang, R., Wang, W., Zhu, Y., Zhang, H., Zhao, W., 2015. Natural *β*-dihydroagarofuran-type sesquiterpenoids as cognition-enhancing and neuroprotective agents from medicinal plants of the genus *Celastrus*. J. Nat. Prod. 78, 2175–2186. https://doi.org/10.1021/acs.jnatprod.5b00234.

Ning, R., Mu, H., Cen, L., Wang, T., Xu, X., He, S., Jiang, M., Zhao, W., 2022. First report on inhibitory effect against osteoclastogenesis of dihydro-*β*-agarofuran-type sesquiterpenoids. J. Agric. Food Chem. 70, 554–566. https://doi.org/10.1021/acs.jafc.1c06862.

Nothias, L.F., Nothias-Esposito, M., da Silva, R., Wang, M., Protsyuk, I., Zhang, Z., Sarvepalli, A., Leyssen, P., Touboul, D., Costa, J., Paolini, J., Alexandrov, T., Litaudon, M., Dorrestein, P.C., 2018. Bioactivity-based molecular networking for the discovery of drug leads in natural product bioassay-guided fractionation. J. Nat. Prod. 81, 758–767. https://doi.org/10.1021/acs.jnatprod.7b00737.

Nothias, L.F., Petras, D., Schmid, R., Duhrkop, K., Rainer, J., Sarvepalli, A., Protsyuk, I., Ernst, M., Tsugawa, H., Fleischauer, M., Aicheler, F., Aksenov, A.A., Alka, O., Allard, P.M., Barsch, A., Cachet, X., Caraballo-Rodriguez, A.M., Da Silva, R.R., Dang, T., Garg, N., Gauglitz, J.M., Gurevich, A., Isaac, G., Jarmusch, A.K., Kameník, Z., Kang, K.B., Kessler, N., Koester, I., Korf, A., Le Gouellec, A., Ludwig, M., Martin, H.C., McCall, L.I., McSayles, J., Meyer, S.W., Mohimani, H., Morsy, M., Moyne, O., Neumann, S., Neuweger, H., Nguyen, N.H., Nothias-Esposito, M., Paolini, J., Phelan, V.V., Pluskal, T., Quinn, R.A., Rogers, S., Shrestha, B., Tripathi, A., van der Hooft, J.J.J., Vargas, F., Weldon, K.C., Witting, M., Yang, H., Zhang, Z., Zubeil, F., Kohlbacher, O., Böcker, S., Alexandrov, T., Bandeira, N., Wang, M., Dorrestein, P.C., 2020. Feature-based molecular networking in the GNPS analysis environment. Nat. Methods 17, 905–908. https://doi.org/10.1038/s41592-020-0933-6.

Nunez, M.J., Jiménez, I.A., Mendoza, C.R., Chavez-Sifontes, M., Martinez, M.L., Ichiishi, E., Tokuda, R., Tokuda, H., Bazzocchi, I.L., 2016. Dihydro-*β*-agarofuran sesquiterpenes from celastraceae species as anti-tumour-promoting agents: structure-activity relationship. Eur. J. Med. Chem. 111, 95–102. https://doi.org/10.1016/j.ejmech.2016.01.049.

Pluskal, T., Castillo, S., Villar-Briones, A., Oresic, M., 2010. MZmine 2: modular framework for processing, visualizing, and analyzing mass spectrometry-based molecular profile data. BMC Bioinf. 11, 395. https://doi.org/10.1186/1471-2105-11-395.

Quinn, R.A., Nothias, L.F., Vining, O., Meehan, M., Esquenazi, E., Dorrestein, P.C., 2017. Molecular networking as a drug discovery, drug metabolism, and precision medicine strategy. Trends Pharmacol. Sci. 38, 143–154. https://doi.org/10.1016/j.tips.2016.10.011.

Shannon, P., Markiel, A., Ozier, O., Baliga, N.S., Wang, J.T., Ramage, D., Amin, N., Schwikowski, B., Ideker, T., 2003. Cytoscape: a software environment for integrated models of biomolecular interaction networks. Genome Res. 13, 2498–2504. https://doi.org/10.1101/gr.1239303.

Sheldrick, G.M., 2015. Crystal structure refinement with SHELXL. Acta Crystallogr. C: Struct. Chem. 71, 3–8. https://doi.org/10.1107/S2053229614024218.

Spek, A.L., 2015. Platon squeeze: a tool for the calculation of the disordered solvent contribution to the calculated structure factors. Acta Crystallogr. C: Struct. Chem. 71, 9–18. https://doi.org/10.1107/S2053229614024929.

Takaishi, Y., Noguchi, H., Murakami, K., Nakano, K., Tomimatsu, T., 1990. Sesquiterpene esters, triptogelin A-1-A-4, from *Tripterygium wilfordii* var. *regelii*. Phytochemistry 29, 3869–3873. https://doi.org/10.1016/0031-9422(90)85349-K.

Takaishi, Y., Ohshima, S., Nakano, K., Tomimatsu, T., Tokuda, H., Nishino, H., Iwashima, A., 1993. Structures of sesquiterpene polyol esters from *Celastrus stephanotiifolius* with potential tumor-promotion inhibitory activity. J. Nat. Prod. 56, 815–824. https://doi.org/10.1021/np50096a003.

Takaishi, Y., Tokura, K., Tamai, S., Ujita, K., Nakano, K., Tomimatsu, T., 1991. Sesquiterpene polyol esters from *Tripterygium wilfordii* var. *regelii*. Phytochemistry 30. https://doi.org/10.1016/0031-9422(91)84210-J, 1567–1562.

Torres-Romero, D., Muñoz-Martínez, F., Jiménez, I.A., Castanys, S., Gamarro, F., Bazzocchi, I.L., 2009. Novel dihydro-β-agarofuran sesquiterpenes as potent modulators of human P-glycoprotein dependent multidrug resistance. Org. Biomol. Chem. 7, 5166–5172. https://doi.org/10.1039/B915678J.

Tu, Y.Q., Hu, Y.J., Wu, W.J., Chen, N.Y., Pan, X.P., 1992. Sesquiterpene polyol esters from *Celastrus angulatus*. Phytochemistry 31, 3633–3634. https://doi.org/10.1016/0031-9422(92)83743-I.

Wang, M., Carver, J.J., Phelan, V.V., Sanchez, L.M., Garg, N., Peng, Y., Nguyen, D.D., Watrous, J., Kapono, C.A., Luzzatto-Knaan, T., Porto, C., Bouslimani, A., Melnik, A. V., Meehan, M.J., Liu, W.T., Crüsemann, M., Boudreau, P.D., Esquenazi, E., Sandoval-Calderon, M., Kersten, R.D., Pace, L.A., Quinn, R.A., Duncan, K.R., Hsu, C. C., Floros, D.J., Gavilan, R.G., Kleigrewe, K., Northen, T., Dutton, R.J., Parrot, D., Carlson, E.E., Aigle, B., Michelsen, C.F., Jelsbak, L., Sohlenkamp, C., Pevzner, P., Edlund, A., McLean, J., Piel, J., Murphy, B.T., Gerwick, L., Liaw, C.C., Yang, Y.L., Humpf, H.U., Maansson, M., Keyzers, R.A., Sims, A.C., Johnson, A.R., Sidebottom, A. M., Sedio, B.E., Klitgaard, A., Larson, C.B., Boya, C.A.P., Torres-Mendoza, D., Gonzalez, D.J., Silva, D.B., Marques, L.M., Demarque, D.P., Pociute, E., O'Neill, E.C., Briand, E., Helfrich, E.J.N., Granatosky, E.A., Glukhov, E., Ryffel, F., Houson, H., Mohimani, H., Kharbush, J.J., Zeng, Y., Vorholt, J.A., Kurita, K.L., Charusanti, P., McPhail, K.L., Nielsen, K.F., Vuong, L., Elfeki, M., Traxler, M.F., Engene, N., Koyama, N., Vining, O.B., Baric, R., Silva, R.R., Mascuch, S.J., Tomasi, S., Jenkins, S., Macherla, V., Hoffman, T., Agarwal, V., Williams, P.G., Dai, J., Neupane, R., Gurr, J., Rodríguez, A.M.C., Lamsa, A., Zhang, C., Dorrestein, K., Duggan, B.M., Almaliti, J., Allard, P.M., Phapale, P., Nothias, L.F., Alexandrov, T., Litaudon, M., Wolfender, J. L., Kyle, J.E., Metz, T.O., Peryea, T., Nguyen, D.T., VanLeer, D., Shinn, P., Jadhav, A., Müller, R., Waters, K.M., Shi, W., Liu, X., Zhang, L., Knight, R., Jensen, P.R., Palsson, B., Pogliano, K., Linington, R.G., Gutiérrez, M., Lopes, N.P., Gerwick, W.H., Moore, B.S., Dorrestein, P.C., Bandeira, N., 2016. Sharing and community curation of mass spectrometry data with global natural products social molecular networking. Nat. Biotechnol. 34, 828–837. https://doi.org/10.1038/nbt.3597.

Wavefunction Inc, 2013. Spartan '14 (Irvine, CA, USA).

Wibowo, M., Levrier, C., Sadowski, M.C., Nelson, C.C., Wang, Q., Holst, J., Healy, P.C., Hofmann, A., Davis, R.A., 2016. Bioactive dihydro-β-agarofuran sesquiterpenoids from the Australian rainforest plant *Maytenus bilocularis*. J. Nat. Prod. 79, 1445–1453.

Wu, D.G., Liu, J.K., Cheng, C.Q., 1992. Angulatueoid G and H, sesquiterpenes from the seeds of *Celastrus angulatus*. Phytochemistry 31, 4219–4222. https://doi.org/10.1021/acs.jnatprod.6b00190.

Xu, J., Jin, D., Zhao, P., Song, X., Sum, Z., Guo, Y., Zhan, L., 2012. Sesquiterpenes inhibiting NO production from *Celastrus orbiculatus*. Fitoterapia 83, 1302–1305. https://doi.org/10.1016/j.fitote.2011.12.026.

Yun, C.Y., Ko, S.M., Choi, Y.P., Kim, B.J., Lee, J., Kim, J.M., Kim, J.Y., Song, J.Y., Kim, S. H., Hwang, B.Y., Hong, J.T., Han, S.B., Kim, Y., 2018. α-Viniferin improves facial hyperpigmentation via accelerating feedback termination of cAMP/PKA-signaled phosphorylation circuit in facultative melanogenesis. Theransotics 8, 2031–2043. https://doi.org/10.7150/thno.24385.

Zheng, H., Wu, J., Liu, D., Zhang, Z., Ye, R., Li, R., Chen, X., 2021. Bioactive dihydroagarofuran sesquiterpenes from the twigs of *Tripterygium hypoglaucum*. Phytochem. Lett. 41, 92–100. https://doi.org/10.1016/j.phytol.2020.10.011.

Zhou, J., Han, N., Lv, G., Jia, L., Liu, Z., Yin, J., 2017. Two new β-dihydroagarofuran sesquiterpenes from *Celastrus orbiculatus* Thunb and their anti-proliferative activity. Molecules 22, 948–958. https://doi.org/10.3390/molecules22060948.

Zhu, Y., Miao, Z., Ding, J., Zhao, W., 2008. Cytotoxic dihydroagarofuranoid sesquiterpenes from the seeds of *Celastrus orbiculatus*. J. Nat. Prod. 71, 1005–1010. https://doi.org/10.1021/np800052d.